SMC protein RecN drives RecA filament translocation and remodelling for *in vivo* homology search

Afroze Chimthanawala, Jyotsana J Parmar, Sujan Kumar, Krishnan S. Iyer, Madan Rao*, Anjana Badrinarayanan*

National Centre for Biological Sciences (TIFR), Bengaluru 560065, India

*To whom correspondence should be addressed; E-mail: madan@ncbs.res.in, anjana@ncbs.res.in

While the molecular repertoire of the homologous recombination pathway is well-studied, the search mechanism that enables recombination between distant homologous regions is poorly understood. Earlier work suggests that the recombinase RecA, an essential component for homology search, forms an elongated filament, nucleating at the break site. How this RecA structure carries out long distance search remains unclear. Here, we follow the dynamics of RecA after induction of a single double-strand break on the Caulobacter chromosome. We find that the RecA-nucleoprotein filament, once formed, rapidly translocates in a directional manner in the cell, undergoing several pole-to-pole traversals, until homology search is complete. Concomitant with translocation, we observe dynamic remodelling of the filament. Importantly in vivo, the RecA filament alone is incapable of such long distance movement; both translocation and dynamic remodelling are contingent on action of SMC-like protein RecN, via its ATPase cycle. We provide a stochastic description of RecN-regulated changes in filament length during translocation via modulation of RecA assembly-disassembly. In summary, we have uncovered the three key elements of homology search driven by RecN: mobility of a finite segment of RecA, filament remodelling and ability to conduct multiple pole-to-pole traversals, which together point to a novel optimal search strategy.

Keywords: homology search, homologous recombination, double-strand break, bacteria, RecA, Structural Maintenance of Chromosome proteins, RecN, live-cell imaging, stochastic dynamics, assembly-disassembly

Introduction

DNA double-strand breaks (DSBs), if left unrepaired (or incorrectly repaired) can lead to loss of genetic information, chromosomal rearrangements, mutagenesis and even cell death. Homologous recombination, a process that usually ensures error-free repair of DSBs has emerged as an evolutionarily conserved pathway from bacteria to eukaryotic cells[1,2]. Recent work has shown that recombination-based repair is not only local, such as during post-replicative cohesion, but that even distant homologous regions can participate in such repair[2–12]. This is particularly relevant for bacteria, where an extensive post-replicative cohesion period is absent[13–19]. Indeed, cells can face DSBs even outside the context of replication (examples include X-rays, IR radiation, chemicals and metabolites such as bleomycin, Topoisomerase dysfunction (from inhibitor action for example), processing of closely-spaced CPDs, endonucleases produced by the cell and bacterial toxins that directly cause DSBs[7,8,20–25]). Several of these breaks rely on recombination-based repair[7,8,21,26,27]. Given the potential lethality associated with unrepaired breaks[7,9,20,21,27–32], it is vital that there be regulatory mechanisms to sense and initiate, translocate and search and finally identify even distant homology regions for repair. These strategies for long distance homology search and repair must potentially depend on the spatial organisation of chromosomes - its extent, geometry and dimensionality[33] - and must involve energy transduction.

In bacteria, for instance, an extensive homology search programme is effected by the highly conserved recombinase, RecA[34–36]. In the first step of the recombination pathway, DSB-ends are processed to reveal ssDNA overhangs, on which RecA can assemble into a filamentous structure[4,37,38] which in turn initiates homology search. *In vitro* studies have shown that RecA molecules in the nucleoprotein filament possess ATPase activity that can influence (a) formation of a continuous filament during RecA loading on ssDNA[39], (b) growth and shrinkage of the filament[40–42], (c) release of the filament from heterologous pairing[35,43], and (d) RecA turnover during strand invasion[42–44]. *In vivo* studies on double-strand break repair have made use of engineered endonuclease-based DSB-inducing systems (such as the I-SceI system) to make targeted breaks on the chromosome and track the associated dynamics[4–6,11,12,45–47]. Using such a system in *E. coli* to study dynamics of long-distance homology search, imaging of RecA has revealed the presence of large assemblies of RecA, described as RecA *filaments* (or 'bundles'), that can even span the length of the cell[5,6]. How this RecA structure carries out homology search is unknown.

In addition, several accessory proteins are reported to modulate the association and turnover of RecA with ssDNA[48,49]. Of these, RecN, a highly conserved repair-associated protein, has been shown to interact with RecA and is essential for DSB repair[49–52]. RecN belongs to the Structural Maintenance of Chromosome (SMC) family of proteins, that play central roles in chromosome dynamics[53]. While their function in chromosome organization and segregation in bacteria has been well-characterized, their role in DNA repair pathways has not been clearly established. Previous studies have suggested a role for RecN in homologous recombination, either via its influence on kinetics of strand-invasion by the RecA filament or by facilitating global chromosomal cohesion between replicated sisters[49,51,54,55]. Indeed the potential relevance of RecN in recombination-based repair is underscored by its extensive conservation with other core recombination-associated proteins such as RuvABC and RecA across bacterial genomes, as well as across domains of life[56].

In conjunction with other molecular regulators, homology search appears to be an efficient and robust process; recent studies reveal that long-distance search and repair can typically be completed within a single generation time of bacterial growth[3,4,6]. How RecA orchestrates this search, the dynamics of the nucleoprotein filament during this process, and the role for RecA regulators in facilitating or modulating homology search, remain largely unknown. To elucidate the mechanism of homology search *in vivo*, we use quantitative live cell imaging to track RecA during DSB repair in the bacterium *Caulobacter crescentus*, together with a theoretical description of RecA dynamics during search.

Here we present evidence for a novel search mechanism involving a RecA nucleoprotein filament that translocates in a directional manner from the break site located at one cell pole, to the opposite cell pole. Unexpectedly, the RecA filament simultaneously undergoes dynamic changes to its structure, while traversing back-and-forth across the length of the cell before finding its homologous partner and initiating homology pairing. Both, large scale movement and dynamic remodelling of RecA are contingent on its association with RecN. We present a stochastic description, where RecN influences dynamic changes in RecA filament lengths via regulation of rates of RecA subunit assembly-disassembly. Such dynamical remodelling and directional movement of the RecA nucleoprotein filament points to a robust mechanism of iterative search, thus enabling recombination between distant sites of homology.

Results

In vivo imaging of RecA reveals key steps of homologous recombination

To follow RecA-dependent search dynamics *in vivo*, we use the I-SceI system developed in *Caulobacter crescentus*[4,38] that allows us to visualize DSB repair between distant homologous regions (Fig. S1A). Briefly, we insert a unique restriction site, *I-SceI*, near the replication origin, which is usually polarly localized in the cell. We induce a DSB by regulated expression of the endonuclease, I-SceI, that cleaves the site to generate a break. We further marked a region of the chromosome near the break-site using fluorescently-tagged MipZ that associates with the origin region. DSB induction results in loss of localization of the MipZ marker close to the break (due to processing of DNA by the helicase-nuclease complex AddAB[4,38]) serving as a reliable proxy to identify cells where only a single copy of the chromosome is cleaved (with only one MipZ marker now being visible). Restoration of the second marker is indicative of repair. Such complete repair events, as reported previously[4], are observed in 30% of all imaged cells during the course of a single experiment (with 22% cells losing both MipZ foci (suggesting two breaks), 18% cells facing no breaks and 30% cells not having completed repair within the imaging window). Using this extensively characterized system[4,38], we follow the process of homology search in two distinct cell types, both blocked for new rounds of replication initiation: pre-divisional cells with two completely replicated and segregated chromosomes (to follow homology search and subsequent recombination-mediated repair of distant homologous regions) and non-replicating swarmer cells with a single chromosome (to follow homology search, without the presence of the homologous repair template)[4,38].

In both cell types, we monitor the dynamics of RecA using live cell imaging of RecA-YFP. Given that endogenously-tagged RecA perturbs the functioning of the protein, we use a well-described strategy in *E. coli,* where RecA is expressed ectopically in a wild type RecA background[4–6,51,57,58]. This strain, as previously described in *Caulobacter*[4], results in RecA-YFP levels being 30-50% of wildtype RecA levels and is found to be comparable to the wild type background in terms of function in generic DNA damage repair and recombination-mediated DSB repair (as assessed via CFU survival measurement on generic as well as DSB-inducing damage). Furthermore: a. RecA-YFP or RecA-mCherry do not localize to the break site in the absence of damage (Fig. S4F) and localize to DSBs only after break processing by AddAB [4]. This is in contrast to RecA tags in *E. coli* that can localize polarly even in the absence

of damage [5,51,57]. b. RecA localization persists only until damage repair. Upon DSB repair (re-emergence of 2 MipZ foci), RecA does not localize in a discrete manner in the cell. This suggests that RecA localization is associated with damage. (Fig. 1A, n=100cells). c. RecA localizes at the site-specific break only. We find that RecA localization correlates with the spatial location of the break site within the cell. (Fig. S2 representative from n=100 cells in each example). d. RecA and RecN colocalize. Both proteins localize only in the presence of DNA damage (Fig. S3A-B, S4F) and we observe them to be colocalized (Fig. S3C). e. Read-out of SOS response (using MMC or Norfloxacin treatment, following previously-described protocols in *Caulobacter*) shows that cells carrying the fluorescently-tagged RecA construct induce the response similar to wild type conditions (Fig. S1D).

We find that *Caulobacter* RecA-YFP forms discrete structures (foci or elongated filaments) only in the presence of DNA damage. In the present study, we use the term 'filament' to describe diffraction-limited RecA localizations. Whether this includes bundles or single filament of RecA polymers[5,6] remains to be determined. In the absence of damage, fluorescence is diffuse throughout the cell (Fig. S4F). We observe three distinct stages following a DSB near the cell pole – (i) *nucleation and growth* of RecA filament near the pole where MipZ localization, proximal to the origin[4,38], is lost (indicating occurrence of a DSB), (ii) *homology search*, where the RecA filament remodels and moves directionally across the length of the cell (expanded in the next sections), and (iii) *repair*, associated with RecA dissociation followed by the reappearance of two distinct MipZ markers (Fig. 1A; top panel shows representative MipZ and RecA images corresponding to each stage (in this case t0 refers to the first time point of imaging. Cells are imaging until 'repair' is complete and two distinct MipZ markers are now visible) and the bottom panel provides quantitation of duration of each stage described, from multiple cells estimated from n = 100 complete repair events).

Growth and directional movement of RecA filament during homology search

We now characterize the dynamics of RecA during the homology search phase. In contrast to the static structures previously reported in *E. coli*[5,6], we find that once RecA nucleates at the DSB site near the pole, it rapidly grows into an elongated filament, following which it dynamically moves across the length of the cell (Fig. 1B, C, S2A, S2D; *Supplementary Video 1*). We follow the time series of the centroid position $x_c(t)$ of the RecA filament along the long-axis of the cell, relative to the cell length L (while analysing traversals, *t0* is defined as the time

154 point prior to the observation of a positive displacement of the RecA localization from the pole
155 at which it first localized (DSB pole); see *Supplementary Results* for details of quantitative
156 analysis). From its initial position $x_c(0)$ close to the nucleation site, we find that the centroid
157 progresses in a stochastic but biased manner, towards the opposite cell pole (Fig. 1D,E). Having
158 reached the opposite cell pole, the RecA filament starts translocating in the reverse direction
159 (Fig. 1C, S2A). Defining a pole-to-pole translocation as a *traversal*, we find that the mean
160 traversal time of the RecA filament is 6 ± 2 min, and typically undergoes multiple traversals
161 (mean = 4) before homology pairing (Fig. 1D).

162 On average, the centroid position is uniformly distributed across the cell length (Fig. 1E, inset).
163 This indicates that there are no hot-spots within the cell that specifically regulate RecA filament
164 dynamics. The distribution of the centroid steps Δx_c, the algebraic difference between the
165 centroid positions at two consecutive time points, exhibits a bias towards positive values,
166 indicating a systematic movement of the RecA filament in one direction. The nonzero weight
167 of this distribution at $\Delta x_c = 0$ is an indication that the RecA filament often stalls (Fig. 1E).

168 Significantly, we observe that when the DNA break is made midcell (+780kb from the origin)[4],
169 the RecA filament nucleates near midcell, and moves towards *either one of the cell poles* (Fig.
170 S2B). Similarly, in non-replicating swarmer cells with a single copy of the chromosome, the
171 RecA filament seems to exhibit interminable pole-to-pole traversals (Fig.2F, S2C;
172 Supplementary Video 2). These observations imply that the homology search dynamics
173 proceeds independent of the homologous repair template. Interestingly, although there are two
174 break ends upon DSB induction, we rarely observed two distinct RecA filaments. Thus, RecA
175 appears to form a single filamentous structure spanning both break ends, which translocates
176 across the cell during homology search.

177 RecN is essential for movement of the RecA filament *in vivo*

178 We now inquire into the molecular basis of the dynamics of the RecA filament during
179 homology search and for holding break ends together during filament translocation. An
180 essential and highly conserved member of the bacterial recombination pathway is the SMC-
181 like protein, RecN[50,52]. However, it still remains unclear as how RecN influences RecA-
182 mediated homologous recombination *in vivo*. Given the universal role of SMC proteins in
183 organizing DNA (for example, via DNA bridging or DNA loop extrusion[53], we asked whether

184 RecN contributed to RecA dynamics and/ or organization of break ends specifically during
185 homology search.

186 Consistent with reports in other bacterial systems[50,52], we find that RecN is essential for
187 successful DSB repair in *Caulobacter*. In absence of *recN* we record no detectable repair
188 events, together with an increased sensitivity to DSB-inducing agents (Fig. S3E–F, S4G). We
189 use the bacterial-two-hybrid system to show that *Caulobacter* RecA and RecN physically
190 interact with each other (Fig. S3D). We also find that the recruitment of RecN to damage sites
191 is RecA dependent (and not only on SOS-dependent expression) (Fig. S3A, B). Furthermore,
192 RecA and RecN are colocalized at a DSB site, with no detectable instances of RecN localizing
193 away from the RecA structure. However, we do observe examples of RecN localizing towards
194 one end of an elongated RecA filament (Fig. S3C).

195 Given these observations, we investigate how RecN impacts RecA dynamics and homology
196 search. For this, we first delete *recN* and follow the dynamics of RecA during the search
197 process via live-cell imaging. As in case of wild type, we still observe a single RecA
198 localization in *recN* cells, suggesting that RecN does not contribute to holding break ends
199 together. Instead, we find that upon *recN* deletion, the RecA filament ceases to translocate in
200 pre-divisional cells (Fig. 2A-D; *Supplementary Video 3*) (here, *t0* is defined as the first time
201 point when a RecA localization is observed). Unlike wild type, the RecA filament remains
202 rooted to the pole where the break occurred (Fig. 2B, C, D (inset)) and does not undergo pole-
203 to-pole traversal over the entire course of imaging, up to 100 min (Fig. 2C). Concomitantly, no
204 RecA dissociation is observed, consistent with the idea that recombination between distant
205 homologous regions involves RecN-driven RecA movement. In our experiments, all repair
206 events are associated with the formation and mobility of RecA filaments (and search across the
207 cell). Lack of search (as seen with the absence of RecN) results in 0 repair events (Fig. S4G).

208 We find a similar effect on the RecA filament translocation in the absence of *recN*, in non-
209 replicating swarmer cells with only a single copy of the chromosome, in support of our
210 assertion that RecN-driven RecA movement for homology search occurs independent of a
211 homologous template for repair (Fig. 2E, F; *Supplementary Video 4*). Finally, these
212 perturbations to RecA dynamics are observed only in cells lacking the repair-specific SMC-
213 like protein (RecN) and not the SMC protein (Smc) involved in chromosome organization and
214 segregation in non-damage conditions[53] (Fig. S3F, G).

To study which aspects of RecA activity is perturbed in the absence of *recN*, we assess the effects of *recN* deletion on kinetic rates at different stages of the RecA dynamics. In the nucleation stage, we measure the time taken from MipZ disappearance to the appearance of a RecA nucleation event at a DSB site, and find it comparable to wild type cells (Fig. S4A). In the growth stage following nucleation (and prior to search), we find that the initial rates of RecA loading are unaltered in *recN* deleted cells (Fig. S4D, E). In line with this, we observe that the frequency of RecA nucleation events across *recN* cells is comparable to wild type, even under generic mitomycin-C (MMC) damage (Fig. S4F).

Finally, we examine whether the absence of RecA filament movement in *recN* deleted cells is a consequence of a RecA filament instability. Previous studies have shown that cells lacking *recA* or with mutants of RecA that are unable to stably associate with a DSB, undergo 'rec-less' degradation, resulting in excessive loss of DNA around a break site[34,59]. Hence we measure DNA degradation in cells with a single DSB (+780kb from the origin in non-replicating swarmer cells) in wild type, *recA* and *recN* backgrounds, via a deep-sequencing assay[38,60]. Our results show that cells lacking *recN* have degradation profiles that overlap with that of wild type (Fig. S4B, C), while cells lacking *recA* show extensive loss of DNA around the break site. In addition, *recN* deleted cells do not have perturbed SOS induction (Fig. S4H). These observations suggest that RecA filament association with a DSB is not affected in the absence of *recN*, although its movement during homology search is stalled.

RecN-mediated RecA translocation is accompanied by dynamic remodelling of the filament during homology search

Together with the observation that RecN does not affect RecA filament formation at a break site, we find that the average filament lengths are comparable in both wild type and *recN* cells. The length of the RecA filament is typically a small fraction of the cell length and does not extend over the entire cell. In wild type, filament mean fractional length is $\langle l \rangle = 0.2 \pm 0.1$ (Fig. 3E), that corresponds to 1.0 ± 0.5μm for cell lengths that range between 5 - 6μm. In case of *recN* deleted cells, mean fractional length is $\langle l \rangle = 0.2 \pm 0.06$, that corresponds to 1.2 ± 0.5μm for cell lengths that range between 7 - 9μm (*Supplementary Results*). However, although the mean filament lengths are similar, we note that the distribution of Δl, the algebraic difference between the filament lengths at two consecutive time points shows a large range in case of wild

245 type cells (Fig. 3A). This suggests that the filament is dynamically remodelling during
246 translocation, both of which appear to be compromised in the absence of *recN* (Fig. 2D, 3A).

247 Indeed, in wild type cells, we find that directional movement of RecA during homology search
248 is accompanied by dynamic changes in the RecA filament over time. We observe various types
249 of RecA structures in the cell during a traversal, ranging from a focus to extended filamentous
250 structures (Fig. 3B). Importantly, we find no correlation between the length of the RecA
251 filament and its centroid position in the cell (Fig. 3C). Thus, RecN-assisted movement of the
252 RecA filament is accompanied by a stochastic remodelling of its length.

253 How does RecN regulate RecA filament dynamics? The stochastic remodelling of RecA
254 filament length during homology search suggests to us that RecN action must influence
255 assembly-disassembly rates of RecA molecules on the DNA strand (akin to treadmilling)
256 during translocation. Thus, to understand the contribution of assembly-disassembly rates on
257 the observed RecA filament lengths during translocation, we resort to a quantitative stochastic
258 description of the mechanochemistry of RecN-assisted RecA filament dynamics
259 (*Supplementary Results*).

260 In general, the stochastic kinetic model is parameterized by four kinetic rates acting at the ends
261 of the RecA filament (Fig. 3D): a binding rate k^{+} at the left end, a binding rate k^{++} at the right,
262 an unbinding rate k^{-} at the right, and a RecN-dependent unbinding rate k^{--} at the left (noting
263 that the polarity of the filament (and RecA ATPase states) that dictates directionality and
264 assembly-disassembly of RecA molecules[35,40,48,61–63]).

265 We first note that *in vivo*, the levels of RecA (as previously reported[5] and Fig. S4E) and ATP[64]
266 are likely not limiting. With this in mind, if the assembly-disassembly rates are taken to have
267 fixed values, then they cannot be made to balance each other robustly at a particular length and
268 will not give rise to a finite mean filament length at steady state as is observed for wild type
269 (Fig. 3E). One needs a *negative feedback* between the assembly-disassembly rates and the
270 filament length (Fig. 3D, *Supplementary Results*) in order to provide a homeostatic balance
271 leading to a finite mean filament length with small fluctuations about it[65]. We solve this
272 stochastic kinetic model with length dependent rates analytically using a Langevin dynamics
273 with multiplicative noise (*Supplementary Results*). We see that the net bias of the filament to
274 move to the right (Fig. 1E), is contingent on two key features (*Supplementary Results*) - (i) the
275 kinetics rates must violate detailed balance and must thus be driven by energy consumption

276 and (ii) there is a net breaking of left-right symmetry in the binding-unbinding rates, i.e. the
277 net binding at the right end of the filament is larger than the net unbinding at the left end (in
278 the pure assembly-disassembly limit, this is akin to treadmilling[66]).

279 We obtain closed form expressions for the steady state distribution of the filament length P(l)
280 (*Supplementary Results*), which we compare with the observed distribution for the wildtype
281 cells (Fig. 3E). With the disassembly rate k^{-} varying with length as in Fig. 3D, we find that the
282 analytically derived steady state P(l) is a perfect match to the observed distribution (Fig. 3E).
283 In addition, we predict a linear correlation between the mean centroid velocity and mean
284 filament length at steady state, which appears consistent with the wild type data (Fig. 3E
285 (inset)). Thus, our stochastic theory provides a framework for how RecN-mediated regulation
286 of assembly-disassembly rates of RecA subunits within a filament can result in the filament
287 length dynamics observed during homology search.

288 RecN ATPase cycle regulates RecA filament remodelling

289 While the molecular mechanism of filament remodelling and its impact on translocation
290 warrants future investigations (see below), the following additional observation underscores a
291 central role for RecN in modulating RecA filament lengths: A fundamental characteristic of
292 SMC family proteins is their ATPase cycle, that enables them to influence the organization of
293 the substrates they are bound to as well as translocate across large distances within the cell[67–
294 69]. We hence asked how the RecN ATPase cycle regulates RecA filament dynamics, thus
295 facilitating recombination between distant homologous regions. For this, we generate two
296 mutants of RecN in the conserved WalkerA and WalkerB motif that are likely to result in
297 specific perturbation to either ATP binding or ATP hydrolysis properties of RecN[67,70]:
298 *recN*^{D472A} (ATP-binding impaired) and *recN*$^{K35A/E473Q}$ (ATP-hydrolysis impaired)[71]. We find
299 that both mutants are compromised in DNA damage repair, similar to the *recN* deletion (Fig.
300 4C). We next follow the dynamics of RecA during homology search after induction of a DSB
301 in cells carrying either the *recN*^{D472A} or *recN*$^{K35A/E473Q}$ mutations. We find that these mutants
302 also result in static RecA filaments that are unable to translocate across the cell for homology
303 search (Fig. 4A, B, D-F; *Supplementary Video* 5-6). While translocation of RecA is similarly
304 impaired in both mutants, we notice that RecA filament lengths are differently affected. In case
305 of *recN*^{D472A}, RecA filament lengths are comparable to wild type, while they are significantly
306 shorter in the putative RecN ATP hydrolysis mutant (Fig. 4G).

307 Taken together, our observations position RecN early in the recombination pathway,
308 specifically in enabling RecA filament translocation during homology search, with influence
309 on RecA dynamics even in the absence of a homologous repair template. The differential
310 impact of putative RecN ATPase mutants on RecA filament lengths (both resulting in
311 abrogation of translocation), leads us to suggest that RecN, via its ATPase cycle, likely
312 modulates RecA nucleoprotein filament remodelling and drives directional translocation of the
313 filament during homology search.

314 Discussion

315 Using a combination of quantitative live cell imaging and theoretical modelling, we have
316 uncovered a new mechanism for RecA action in long distance homology search during
317 recombination, a fundamental process for the maintenance of life. Our first result is that
318 following a site-specific DSB, RecA nucleates at the DSB site and grows into a nucleoprotein
319 filament which moves in a stochastic but directional manner along the length of the cell, in
320 tandem with RecN. The second main result is that the filament translocation is accompanied
321 by dynamic remodelling of the RecA filament. The dynamic remodelling is a consequence of
322 RecN influenced assembly-disassembly that breaks left-right symmetry (akin to treadmilling)
323 - indeed, a stochastic description of this process agrees remarkably well with quantitative
324 analysis of live cell imaging. The RecA filament makes multiple traversals across the length of
325 the cell before the homologous pair is found, followed by repair. That RecN, via its ATPase
326 cycle, is crucially involved in the search, its termination and subsequent repair is the third main
327 result of the paper.

328 Following our present study, an immediate goal is to deduce the molecular basis of the feed-
329 back regulation that maintains a fixed mean filament length at steady state. Similarly, we will
330 need to unravel the molecular basis of the RecN-regulated dynamics of the RecA nucleoprotein
331 filament. For example, *in vivo* studies in *E. coli* have variably suggested that the DSB-
332 associated RecA structures could either be a bundle[5,58] or a single[6] polymer of RecA molecules.
333 It would be informative to determine the detailed composition of the RecA filament in the
334 present study, along with any impact of RecN on the same. This would require a quantitative
335 characterization of the complete RecA-RecN ATPase cycle, its interaction with the
336 mechanochemistry of the DNA substrate, as well as detailed dissection of the RecA filament
337 architecture.

338 Based on our current observations, we consider two possible scenarios: (A) RecN-mediated
339 regulation of assembly-disassembly rates of RecA molecules in the filament. (B) Motor-driven
340 movement of the RecA nucleoprotein filament and/ or the underlying ssDNA substrate. In line
341 with the possible influence of RecN on mobility of the underlying ssDNA substrate, we find
342 that, in the absence of *recN*, Single-Strand Binding protein (SSB) localization is also restricted
343 to the pole where the break occurs (Fig. S5A). However, pure motor-assisted movement would
344 not be able to explain the stochastic remodelling the filament length, while pure assembly-
345 disassembly, without the dynamics of the DNA, would need to have available a cell-spanning
346 ssDNA segment, which does not appear to be the case in our conditions (Fig. S5A).

347 Thus, we suggest that the RecN-assisted dynamics of the RecA filament could be a
348 consequence of both motor-assisted movement (such as DNA extrusion) and regulation of
349 assembly- disassembly rates of RecA on DNA (via treadmilling). Fig. S5B is our proposed
350 model of the same. Here, RecN action on the DNA could be a consequence of its reported
351 bridging activity of ssDNA (generated around the break-site) with dsDNA[55], thus driving
352 directional movement of RecA, along with its underlying DNA substrate. 'Zipping' refers to
353 RecN action ahead of the translocating RecA filament, while 'extrusion' refers to RecN action
354 behind the filament[72,73].

355 Why does the RecA filament need to undergo dynamic remodelling in addition to movement
356 during homology search? Studies have shown that RecA ATPase rates are stimulated 4-fold
357 upon strand invasion, potentially allowing the RecA filament to release from heterologous
358 pairing during microhomology sampling as well[43]. Separately, RecN has been found to (a)
359 stimulate RecA strand invasion activity[49] and (b) bridge ssDNA and dsDNA[55]. Taken together,
360 it is possible that the RecN-dependent RecA remodelling is a reflection of such microhomology
361 sampling activity prior to homology pairing. The stochasticity of the RecN-driven RecA
362 dynamics and the multiple traversals before identification of the homologous repair template,
363 suggests a novel search mechanism that allows for a regulated genome-wide sampling for
364 homology. Our observations reveal that in addition to the initial waiting time between
365 nucleation to the start of traversals, the translocating RecA filament makes pauses at random
366 intervals. We speculate that RecA molecules might engage in microhomology sampling both
367 initially in the vicinity of the damage site (especially in the post-replicative cohesion period)
368 and during these pause intervals during translocation[43,74].

369 Based primarily on *in vitro* observations, earlier models have suggested that RecA engages in
370 1D sliding movement and intersegment hopping, while regions within the RecA filament
371 engage in microhomology sampling during search[35,74,75]. Our work reveals a central role for
372 regulation of RecA filament dynamics by RecN during long distance search. We uncover the
373 three key elements of this RecN-driven homology search *in vivo*: RecA filament mobility,
374 remodelling of the filament and the ability to undertake multiple pole-to-pole traversals.
375 Together, this suggests a new mechanism of iterative, long distance search within the cell.
376 RecN-mediated multiple pole-to-pole traversals by RecA builds in a kind of *reset* at a fixed
377 spatial location, a strategy that can lead to optimal search[76], thus facilitating repair well within
378 a single generation time of bacterial growth.

379 It is possible that there is some diversity in RecA-dependent long-range homology search
380 dynamics across bacterial systems, to contend with the varying cell shapes, chromosome
381 replication dynamics (multi-fork vs replication only once per cell cycle), and chromosome
382 organization[3–6], thus resulting in static[5,6] or mobile (present study) RecA structures. However,
383 given that RecA and RecN are among the most conserved proteins of the recombination
384 pathway in bacterial genomes and its counterparts are present across domains of life, we believe
385 that the dynamics we describe here is active in other systems as well.

386

Acknowledgements

Authors thank Julia Hitschfel for assistance with bacterial-two-hybrid experiments as well as Meghna Iyer and Varshit Dusad for assistance with developing analysis tools. Authors are grateful to Rodrigo Reyes-Lamothe, David Sherratt, M Srinivasan and AB lab members for feedback and discussion. AB acknowledges support from DST-SERB CRG 2019/003321, HFSP-CDA award (00051/2017) and intramural funding from NCBS-TIFR. JP, SK, KI and MR thank the Simons Foundation for a grant. MR thanks DST-SERB, India for a JC Bose Fellowship.

Materials and Methods

Bacterial strains and growth conditions

Strains, plasmids and oligos used in this study are described in Table S1-S3, respectively. Chromosomal modifications such as integration of fluorescent markers or deletion of genes were performed using the two-step recombination method[77] or with vectors described previously[78]. Transductions were carried out using ΦCr30[79]. Unless otherwise stated, *Caulobacter* cultures were grown at 30°C in peptone yeast extract and supplemented with antibiotics at appropriate concentrations. When growing strains with *dnaA* under an IPTG-inducible promoter, liquid media was supplemented with 0.5 mM IPTG and solid media with 1 mM IPTG. For synchronization experiments, *Caulobacter* cultures were grown till mid-log phase and synchronization protocols were followed as previously described[4]. Protocols used for isolating non-replicating pre-divisional cells and non-replicating swarmer cells[4,38] are briefly described here. For isolation of non-replicating swarmer cells, cultures were grown till mid-log phase in media supplemented with IPTG. Cells were then depleted for DnaA by washing off the inducer and were grown in the absence of IPTG for one generation. This was followed by synchronization and isolation of swarmer cells. These cells were re-suspended in media without IPTG and used for DSB induction experiments. For isolation of non-replicating pre-divisional cells, cultures were grown till mid-log phase in media supplemented with IPTG. Cells were then synchronized and swarmer cells isolated. Swarmers were then released into media lacking IPTG. Cells were then depleted for DnaA by washing off the inducer and grown in the absence of IPTG for one generation. Cell division was blocked via addition of 35 μg/ml cephalexin and these non-replicating pre-divisional cells were further used for DSB induction

417 experiments. In all cases, *recA-YFP* was induced using 0.03% xylose 90 min prior to imaging
418 and subsequently maintained in the agarose pad as well during the entire course of imaging.
419 For imaging SSB-YFP after induction of a break in non-replicating swarmer cells, *ssb-YFP*
420 was induced using 0.03% xylose. DSBs were induced with 2 μM Vanillate. For this, vanillate
421 was added to the growth culture 15 min prior to imaging and was subsequently maintained on
422 the agarose pad as well.

423 Fluorescence Microscopy

424 Time course imaging was performed on 1% agarose pads (Invitrogen ultrapure). For time-lapse
425 imaging, cells were grown on 1.5% GTG agarose pads (low melting) prepared in peptone yeast
426 extract and supplemented with vanillate, xylose or cephalexin at appropriate concentrations
427 and imaged using glass-bottom petri dishes. Imaging was carried out using a wide-field
428 epifluorescence microscope (Eclipse Ti-2E, Nikon) with a 63X oil immersion objective (plan
429 apochromat objective with NA 1.41), illumination from pE4000 light source (CoolLED),
430 Hamamatsu Orca Flash 4.0 camera and a motorized XY stage. During time-lapse imaging,
431 focus was maintained using an infrared-based Perfect Focusing System (Nikon). Image
432 acquisitions were done using NIS-elements software (version 5.1) and images were acquired
433 every 30s, 1 min or 5 min (as indicated in the main text and respective figure legends). For
434 most experiments with RecA, exposure time used for excitation at 490 nm was 400 ms and for
435 550 nm was 500 ms. For imaging MipZ, exposure time used for excitation at 550 nm was 100
436 ms. For imaging YFP expressed from the *sidA* promoter, exposure time used for excitation at
437 490 nm was 500 ms. In all images, scale bars = 2μm. Procedures for image analysis and for
438 extracting key features of RecA localization are described in *Supplementary Results*.

439 DNA degradation assay

440 Implemented as previously described[38]. Briefly, non-replicating swarmer cells with DSB site
441 at +780kb were isolated and released in a media with 0.5 mM Vanillate to induce DSBs.
442 Samples were collected at 0 h (control) and 1 h after DSB induction. Genomic DNA was
443 isolated using DNAeasy blood and tissue kit (Qiagen). Whole genome Illumina sequencing
444 was carried out on the isolated DNA (NGS facility, NCBS, India). Data were further analysed
445 using the following protocol. First, indexing with the reference genome (4.01 Mbp) (NCBI
446 reference sequence:NC-011916.1) was done using BWA[80]. Reads with raw read quality 20
447 were aligned using 'BWAaln –q'. SAMTOOLS (version 0.1.19-96b5f2294a)[80] was used to

448 filter out the multiply-mapped reads. Finally, with BEDTOOLS[81] the read count per bin was
449 calculated using the .bed files containing bin positions. *Caulobacter* genome data obtained
450 after Illumina sequencing, Hiseq 2500 illumina short reads (50 bp), was divided into 1 kb bins.
451 Read counts per bin were normalized to the total reads acquired for that sample. The ratio of
452 normalized reads after DSB (1 h) to normalized reads before DSB (0 h) was plotted to visualize
453 the read enrichment profile obtained across the genome after induction of a DSB. The graph
454 generated was processed further with the Lowess smoothing function in MatLab.

455 ## Bacterial two-hybrid assay

456 Implemented as previously described[38]. Briefly, to investigate physical interaction between a
457 pair of proteins, their respective genes were fused to 3' end of T25 or T18 fragments in pKT or
458 pUT vectors. These vectors were co-transformed into *E. coli* BTH101. Co-transformed cells
459 were grown to saturation in M63 media with maltose and IPTG and 5µl of this culture was
460 spotted on MacConkey agar plates (40 g/L) with maltose, IPTG and appropriate antibiotics.
461 Plates were incubated at 30°C for 2-3 days.

462

References

1. Renkawitz, J., Lademann, C. A. & Jentsch, S. Mechanisms and principles of homology search during recombination. *Nature Reviews Molecular Cell Biology* **15**, 369–383 (2014).
2. Haber, J. E. DNA Repair: The Search for Homology. *BioEssays* **40**, 1700229 (2018).
3. Amarh, V., White, M. A. & Leach, D. R. F. Dynamics of RecA-mediated repair of replication-dependent DNA breaks. *Journal of Cell Biology* **217**, 2299–2307 (2018).
4. Badrinarayanan, A., Le, T. B. K. & Laub, M. T. Rapid pairing and resegregation of distant homologous loci enables double-strand break repair in bacteria. *Journal of Cell Biology* **210**, 385–400 (2015).
5. Lesterlin, C., Ball, G., Schermelleh, L. & Sherratt, D. J. RecA bundles mediate homology pairing between distant sisters during DNA break repair. *Nature* **506**, 249–253 (2014).
6. Wiktor, J. *et al.* RecA finds homologous DNA by reduced dimensionality search. *Nature* **597**, 426–429 (2021).
7. Haber, J. *Genome Stability: DNA Repair and Recombination*. (Garland Science, 2013).
8. Pâques, F. & Haber, J. E. Multiple Pathways of Recombination Induced by Double-Strand Breaks in Saccharomyces cerevisiae. *Microbiol Mol Biol Rev* **63**, 349–404 (1999).
9. Bordelet, H. & Dubrana, K. Keep moving and stay in a good shape to find your homologous recombination partner. *Curr Genet* **65**, 29–39 (2019).
10. Fabre, F. Induced intragenic recombination in yeast can occur during the G1 mitotic phase. *Nature* **272**, 795–798 (1978).
11. Dion, V., Kalck, V., Horigome, C., Towbin, B. D. & Gasser, S. M. Increased mobility of double-strand breaks requires Mec1, Rad9 and the homologous recombination machinery. *Nat Cell Biol* **14**, 502–509 (2012).
12. Miné-Hattab, J. & Rothstein, R. Increased chromosome mobility facilitates homology search during recombination. *Nat Cell Biol* **14**, 510–517 (2012).
13. Kaljević, J. *et al.* Chromosome choreography during the non-binary cell cycle of a predatory bacterium. *Current Biology* **31**, 3707-3720.e5 (2021).
14. Yamaichi, Y., Fogel, M. A. & Waldor, M. K. par genes and the pathology of chromosome loss in Vibrio cholerae. *Proceedings of the National Academy of Sciences* **104**, 630–635 (2007).
15. Ehrle, H. M. *et al.* Polar Organizing Protein PopZ Is Required for Chromosome Segregation in Agrobacterium tumefaciens. *J Bacteriol* **199**, (2017).
16. Dubarry, N., Willis, C. R., Ball, G., Lesterlin, C. & Armitage, J. P. In Vivo Imaging of the Segregation of the 2 Chromosomes and the Cell Division Proteins of Rhodobacter sphaeroides Reveals an Unexpected Role for MipZ. *mBio* **10**, e02515-18 (2019).
17. Jung, A. *et al.* Two-step chromosome segregation in the stalked budding bacterium Hyphomonas neptunium. *Nat Commun* **10**, 3290 (2019).
18. Viollier, P. H. *et al.* Rapid and sequential movement of individual chromosomal loci to specific subcellular locations during bacterial DNA replication. *CELL BIOLOGY* 6 (2004).
19. Le, T. B. K., Imakaev, M. V., Mirny, L. A. & Laub, M. T. High-Resolution Mapping of the Spatial Organization of a Bacterial Chromosome. *Science* (2013) doi:10.1126/science.1242059.
20. Friedberg, E. C. A history of the DNA repair and mutagenesis field: The discovery of base excision repair. *DNA Repair (Amst)* **37**, A35-39 (2016).

21. Li, X. & Heyer, W.-D. Homologous recombination in DNA repair and DNA damage tolerance. *Cell Res* **18**, 99–113 (2008).
22. Cannan, W. J. & Pederson, D. S. Mechanisms and Consequences of Double-Strand DNA Break Formation in Chromatin: DOUBLE-STRAND DNA BREAK FORMATION IN CHROMATIN. *J. Cell. Physiol.* **231**, 3–14 (2016).
23. Bonura, T. & Smith, K. C. Enzymatic production of deoxyribonucleic acid double-strand breaks after ultraviolet irradiation of Escherichia coli K-12. *J Bacteriol* **121**, 511–517 (1975).
24. Bos, J., Yakhnina, A. A. & Gitai, Z. BapE DNA endonuclease induces an apoptotic-like response to DNA damage in Caulobacter. *PNAS* **109**, 18096–18101 (2012).
25. Nesić, D., Hsu, Y. & Stebbins, C. E. Assembly and function of a bacterial genotoxin. *Nature* **429**, 429–433 (2004).
26. Resnick, M. A. The repair of double-strand breaks in DNA: A model involving recombination. *Journal of Theoretical Biology* **59**, 97–106 (1976).
27. Kowalczykowski, S., Hunter, N. & Heyer, W.-D. *DNA Recombination*. (CSH Press, 2016).
28. Bennett, C. B., Lewis, A. L., Baldwin, K. K. & Resnick, M. A. Lethality induced by a single site-specific double-strand break in a dispensable yeast plasmid. *Proceedings of the National Academy of Sciences* **90**, 5613–5617 (1993).
29. Featherstone, C. & Jackson, S. P. DNA double-strand break repair. *Current Biology* **9**, R759–R761 (1999).
30. Mehta, A., Beach, A. & Haber, J. E. Homology Requirements and Competition between Gene Conversion and Break-Induced Replication during Double-Strand Break Repair. *Molecular Cell* **65**, 515-526.e3 (2017).
31. Elango, R. *et al.* Break-induced replication promotes formation of lethal joint molecules dissolved by Srs2. *Nat Commun* **8**, 1790 (2017).
32. Trenner, A. & Sartori, A. A. Harnessing DNA Double-Strand Break Repair for Cancer Treatment. *Front Oncol* **9**, 1388 (2019).
33. Bénichou, O., Loverdo, C., Moreau, M. & Voituriez, R. Intermittent search strategies. *Rev. Mod. Phys.* **83**, 81–129 (2011).
34. Willetts, N. S. & Clark, A. J. Characteristics of Some Multiply Recombination-Deficient Strains of *Escherichia coli*. *J Bacteriol* **100**, 231–239 (1969).
35. Bell, J. C. & Kowalczykowski, S. C. RecA: Regulation and Mechanism of a Molecular Search Engine. *Trends in Biochemical Sciences* **41**, 491–507 (2016).
36. Cox, M. M. Regulation of Bacterial RecA Protein Function. *Critical Reviews in Biochemistry and Molecular Biology* **42**, 41–63 (2007).
37. Smith, G. R. How RecBCD Enzyme and Chi Promote DNA Break Repair and Recombination: a Molecular Biologist's View. *Microbiology and Molecular Biology Reviews* **76**, 217–228 (2012).
38. Badrinarayanan, A., Le, T. B. K., Spille, J.-H., Cisse, I. I. & Laub, M. T. Global analysis of double-strand break processing reveals in vivo properties of the helicase-nuclease complex AddAB. *PLoS Genet* **13**, e1006783 (2017).
39. Kim, S. H. *et al.* RecA filament maintains structural integrity using ATP-driven internal dynamics. *Sci. Adv.* **3**, e1700676 (2017).
40. Kim, S. H. *et al.* Cooperative Conformational Transitions Keep RecA Filament Active During ATPase Cycle. *J. Am. Chem. Soc.* **136**, 14796–14800 (2014).
41. van Loenhout, M. T. J., van der Heijden, T., Kanaar, R., Wyman, C. & Dekker, C. Dynamics of RecA filaments on single-stranded DNA. *Nucleic Acids Research* **37**, 4089–4099 (2009).

42. Cox, J. M., Tsodikov, O. V. & Cox, M. M. Organized Unidirectional Waves of ATP Hydrolysis within a RecA Filament. *PLoS Biol* **3**, e52 (2005).
43. Lee, J. Y., Qi, Z. & Greene, E. C. ATP hydrolysis Promotes Duplex DNA Release by the RecA Presynaptic Complex. *Journal of Biological Chemistry* **291**, 22218–22230 (2016).
44. Lindsley, J. E. & Cox, M. M. Assembly and disassembly of RecA protein filaments occur at opposite filament ends. Relationship to DNA strand exchange. *Journal of Biological Chemistry* **265**, 9043–9054 (1990).
45. Unal, E., Heidinger-Pauli, J. M. & Koshland, D. DNA double-strand breaks trigger genome-wide sister-chromatid cohesion through Eco1 (Ctf7). *Science* **317**, 245–248 (2007).
46. Tripuraneni, V. *et al.* Local nucleosome dynamics and eviction following a double-strand break are reversible by NHEJ-mediated repair. *Genome Res.* gr.271155.120 (2021) doi:10.1101/gr.271155.120.
47. Charpentier, M. *et al.* CtIP fusion to Cas9 enhances transgene integration by homology-dependent repair. *Nat Commun* **9**, 1133 (2018).
48. Bell, J. C., Plank, J. L., Dombrowski, C. C. & Kowalczykowski, S. C. Direct imaging of RecA nucleation and growth on single molecules of SSB-coated ssDNA. *Nature* **491**, 274–278 (2012).
49. Uranga, L. A., Reyes, E. D., Patidar, P. L., Redman, L. N. & Lusetti, S. L. The cohesin-like RecN protein stimulates RecA-mediated recombinational repair of DNA double-strand breaks. *Nat Commun* **8**, 15282 (2017).
50. Picksley, S. M., Attfield, P. V. & Lloyd, R. G. Repair of DNA double-strand breaks in Escherichia coli K12 requires a functional recN product. *Mol Gen Genet* **195**, 267–274 (1984).
51. Vickridge, E., Planchenault, C., Cockram, C., Junceda, I. G. & Espéli, O. Management of E. coli sister chromatid cohesion in response to genotoxic stress. *Nat Commun* **8**, 14618 (2017).
52. Klimova, A. N. & Sandler, S. J. An Epistasis Analysis of recA and recN in Escherichia coli K-12. *Genetics* **216**, 381–393 (2020).
53. Nolivos, S. & Sherratt, D. The bacterial chromosome: architecture and action of bacterial SMC and SMC-like complexes. *FEMS Microbiol Rev* **38**, 380–392 (2014).
54. Reyes, E. D., Patidar, P. L., Uranga, L. A., Bortoletto, A. S. & Lusetti, S. L. RecN Is a Cohesin-like Protein That Stimulates Intermolecular DNA Interactions in Vitro. *Journal of Biological Chemistry* **285**, 16521–16529 (2010).
55. Keyamura, K. & Hishida, T. Topological DNA-binding of structural maintenance of chromosomes-like RecN promotes DNA double-strand break repair in Escherichia coli. *Commun Biol* **2**, 413 (2019).
56. Rocha, E. P. C., Cornet, E. & Michel, B. Comparative and Evolutionary Analysis of the Bacterial Homologous Recombination Systems. *PLoS Genet* **1**, e15 (2005).
57. Renzette, N. *et al.* Localization of RecA in Escherichia coli K-12 using RecA–GFP. *Molecular Microbiology* **57**, 1074–1085 (2005).
58. Rajendram, M. *et al.* Anionic Phospholipids Stabilize RecA Filament Bundles in Escherichia coli. *Molecular Cell* **60**, 374–384 (2015).
59. Kuzminov, A. & Stahl, F. W. Stability of linear DNA in recA mutant Escherichia coli cells reflects ongoing chromosomal DNA degradation. *J Bacteriol* **179**, 880–888 (1997).
60. Wiktor, J., van der Does, M., Büller, L., Sherratt, D. J. & Dekker, C. Direct observation of end resection by RecBCD during double-stranded DNA break repair in vivo. *Nucleic Acids Research* **46**, 1821–1833 (2018).
61. Joo, C. *et al.* Real-Time Observation of RecA Filament Dynamics with Single Monomer Resolution. *Cell* **126**, 515–527 (2006).

608 62. Bork, J. M., Cox, M. M. & Inman, R. B. RecA Protein Filaments Disassemble in the
609 5′ to 3′ Direction on Single-stranded DNA*. *Journal of Biological Chemistry* **276**, 45740–
610 45743 (2001).
611 63. Shan, Q., Bork, J. M., Webb, B. L., Inman, R. B. & Cox, M. M. RecA protein
612 filaments: end-dependent dissociation from ssDNA and stabilization by RecO and RecR
613 proteins. *J Mol Biol* **265**, 519–540 (1997).
614 64. Barbé, J., Villaverde, A. & Guerrero, R. Evolution of cellular ATP concentration after
615 UV-mediated induction of SOS system in Escherichiacoli. *Biochemical and Biophysical*
616 *Research Communications* **117**, 556–561 (1983).
617 65. Mohapatra, L., Goode, B. L., Jelenkovic, P., Phillips, R. & Kondev, J. Design
618 Principles of Length Control of Cytoskeletal Structures. *Annu. Rev. Biophys.* **45**, 85–116
619 (2016).
620 66. Howard, J. & Clark, R. Mechanics of Motor Proteins and the Cytoskeleton. *Applied*
621 *Mechanics Reviews* **55**, B39–B39 (2002).
622 67. Badrinarayanan, A., Reyes-Lamothe, R., Uphoff, S., Leake, M. C. & Sherratt, D. J. In
623 Vivo Architecture and Action of Bacterial Structural Maintenance of Chromosome Proteins.
624 *Science* **338**, 528–531 (2012).
625 68. Diebold-Durand, M.-L. *et al.* Structure of Full-Length SMC and Rearrangements
626 Required for Chromosome Organization. *Molecular Cell* **67**, 334-347.e5 (2017).
627 69. Wilhelm, L. *et al.* SMC condensin entraps chromosomal DNA by an ATP hydrolysis
628 dependent loading mechanism in Bacillus subtilis. *eLife* **4**, e06659 (2015).
629 70. Arumugam, P. *et al.* ATP hydrolysis is required for cohesin's association with
630 chromosomes. *Curr Biol* **13**, 1941–1953 (2003).
631 71. Pellegrino, S. *et al.* Structural and Functional Characterization of an SMC-like Protein
632 RecN: New Insights into Double-Strand Break Repair. *Structure* **20**, 2076–2089 (2012).
633 72. Wang, X. *et al.* In Vivo Evidence for ATPase-Dependent DNA Translocation by the
634 Bacillus subtilis SMC Condensin Complex. *Molecular Cell* **71**, 841-847.e5 (2018).
635 73. Brandão, H. B., Ren, Z., Karaboja, X., Mirny, L. A. & Wang, X. DNA-loop-extruding
636 SMC complexes can traverse one another in vivo. *Nat Struct Mol Biol* **28**, 642–651 (2021).
637 74. Forget, A. L. & Kowalczykowski, S. C. Single-molecule imaging of DNA pairing by
638 RecA reveals a three-dimensional homology search. *Nature* **482**, 423–427 (2012).
639 75. Ragunathan, K., Liu, C. & Ha, T. RecA filament sliding on DNA facilitates homology
640 search. *eLife* **1**, e00067 (2012).
641 76. Evans, M. R., Majumdar, S. N. & Schehr, G. Stochastic resetting and applications. *J.*
642 *Phys. A: Math. Theor.* **53**, 193001 (2020).
643 77. Skerker, J. M., Prasol, M. S., Perchuk, B. S., Biondi, E. G. & Laub, M. T. Two-
644 Component Signal Transduction Pathways Regulating Growth and Cell Cycle Progression in
645 a Bacterium: A System-Level Analysis. *PLoS Biol* **3**, e334 (2005).
646 78. Thanbichler, M., Iniesta, A. A. & Shapiro, L. A comprehensive set of plasmids for
647 vanillate- and xylose-inducible gene expression in Caulobacter crescentus. *Nucleic Acids*
648 *Research* **35**, e137–e137 (2007).
649 79. Ely, B. [17] Genetics of Caulobacter crescentus. in *Methods in Enzymology* vol. 204
650 372–384 (Academic Press, 1991).
651 80. Li, H. & Durbin, R. Fast and accurate short read alignment with Burrows-Wheeler
652 transform. *Bioinformatics* **25**, 1754–1760 (2009).
653 81. Quinlan, A. R. & Hall, I. M. BEDTools: a flexible suite of utilities for comparing
654 genomic features. *Bioinformatics* **26**, 841–842 (2010).

655

656 # Figure Legends

657 **Fig. 1. Dynamics of RecA filament during homologous recombination.** (A) Montage of key
658 events of homologous recombination observed via live-cell imaging of both break/ homology
659 site (MipZ; red) as well as DSB dynamics (RecA; green). Top panel shows representative cell
660 examples for each stage (t0 refers to the first time point of imaging; bottom panel provides
661 quantitative estimation of duration of the key events described across multiple cells (n = 100
662 repair events). Single DSB induction (white asterisk) is marked by the disappearance of one of
663 the two MipZ localizations. *RecA nucleation* is defined as the period between DSB induction
664 and the initiation of RecA localization at the break site, followed by *homology search*, marked
665 by the translocation of the RecA filament in the cell. *Repair* is marked by the loss of RecA
666 filament after search, followed by the reappearance of two MipZ markers. The time line below
667 shows the period of RecA nucleation and loading (after break induction), homology search and
668 repair (n = 100). Scale bar: 2 μm here and in all other images. (B) Montage of RecA-YFP
669 tracked over time (duration of a single pole-to-pole traversal event) after induction of a single
670 DSB during homology search (white asterisk). Here, *t0* is defined as the time point prior to the
671 observation of a positive displacement of the RecA localization from the pole at which it first
672 localized (DSB pole) (C) Representative RecA-YFP fluorescence profiles across [top] one
673 pole-to-pole traversal and [bottom] multiple traversals. (D) Centroid position of the RecA
674 filament x_c (measured relative to cell length) versus time over a single traversal. Plot shows
675 mean and standard deviation from data collected over n = 99 cells. Mean traversal time $t = 6 \pm$
676 2 min is indicated. (E) Bar graph representing the probability distribution of the centroid steps
677 Δx_c, (i.e. the algebraic difference between the centroid positions at two consecutive time points
678 (60 sec apart)), shows a bias towards positive values and a weight at $\Delta x_c = 0$ (Error bars
679 represent sample error). [inset] Bar graph representing the probability distribution of x_c taken
680 over a single traversal cycle (n = 795). All data shown are from pre-divisional cells.

681 **Fig. 2. RecN is essential for RecA filament movement *in vivo*.** (A) Montage of RecA-YFP
682 tracked over multiple pole-to-pole traversal events after induction of a single DSB (white
683 asterisk) - [top] in wild type, [bottom] in cells lacking *recN* (for the same duration as wild type
684 cells above). Here, *t0* is defined as the first time point when a RecA localization is observed.
685 Examples shown from pre-divisional cells. (B) Representative RecA-YFP fluorescence
686 profiles in a *recN* deletion background. [top] RecA is tracked for the expected duration of two
687 pole-to-pole traversals; [bottom] over expected duration of multiple traversals. Data shown are

688 from pre-divisional cells. (C) Centroid position of the RecA filament x_c versus time for cells
689 lacking *recN*. Plot shows mean and standard deviation from data collected over n = 50 cells.
690 Data shown are from pre-divisional cells. (D) Probability distribution of the centroid steps Δx_c
691 shows no bias (Error bars represent sample error). [inset] Probability distribution of x_c taken
692 over all time points (n = 852), in cells lacking *recN*. Data shown are from pre-divisional cells.
693 (E) Representative RecA-YFP fluorescence profile in a *recN* deletion background. DSB is
694 induced in non-replicating swarmer cells with a single chromosome, thus lacking a
695 homologous template for repair. (F) Probability distribution of x_c in wild type (n = 911) and
696 cells lacking *recN* (n = 1039). DSB is induced in non-replicating swarmer cells with a single
697 chromosome, thus lacking a homologous template for repair.

698 **Fig. 3. RecN-mediated RecA translocation is accompanied by dynamic remodelling of the**
699 **filament during homology search.** (A) Probability distribution of the length changes Δl, (i.e.
700 the algebraic difference between the filament lengths at two consecutive time points (60 sec
701 apart)) in wild type (n = 347) and cells lacking *recN* (n = 750). Error bars represent sample
702 error. Data shown are from pre-divisional cells. (B) Representative images of the types of RecA
703 localizations observed during a wild type traversal, with (1, 2) showing *puncta* and (3 - 9)
704 showing *extended filamentous* structures. Data shown are from pre-divisional cells. (C) Joint
705 probability distribution of l and x_c taken over a single traversal in wild type cells (n = 795).
706 Data shown are from pre-divisional cells. (D) (top) Stochastic kinetic description of RecN-
707 assisted dynamics of RecA filament in terms of its centroid position and length measured in
708 the lab frame. The rates of assembly and disassembly at the two ends of the filament are shown.
709 (bottom) To maintain a finite mean length, the rates of disassembly must exceed the assembly
710 rates at large l (*Supplementary Results*). Choosing the disassembly rate k^- to be linear in l, and
711 the other rates being constant, allows us to match analytically derived length distribution to the
712 experimentally measured one. (E) The analytically derived distribution P(l) (green)
713 (*Supplementary Results*) is compared with the experimental data for wild type (plotted as a
714 density histogram) (fit parameters presented in the *Supplementary Results*). [inset] The theory
715 predicts a relation between the centroid velocity v_c and mean filament length $\langle l \rangle$. Dashed red
716 line highlights the relationship between v_c and $\langle l \rangle$, estimated Pearson correlation coefficient r
717 = 0.236 (p-value = 0.045, 95% CI [0.00597689, 0.441833]) (for this estimate we have excluded
718 outliers).

719 **Fig. 4. RecN ATPase cycle regulates RecA filament dynamics.** (A) Montage of RecA- YFP
720 tracked over time after induction of a single DSB (white asterisk) for putative RecN ATP
721 hydrolysis mutant (*recN*$^{K35A/E473Q}$). (B) Representative montage of RecA-YFP tracked over
722 time after induction of a single DSB (white asterisk) for putative RecN ATP binding mutant
723 (*recN*^{D472A}). (C) Sensitivity of *recN*^{D472A} and *recN*$^{K35A/E473Q}$ to DSB-inducing agent norfloxacin
724 is evaluated (in comparison to wild type, Δ*recN* and Δ*recA* cells, from Fig. S3E).
725 Representative image from at least three independent repeats. (D) [top] Representative RecA-
726 YFP fluorescence profile across the length of the cell in a *recN*$^{K35A/E473Q}$ background. [bottom]
727 Representative RecA-YFP fluorescence profile across the length of the cell in a *recN*^{D472A}
728 background. (E) Position of centroid of RecA filament normalized to length of the cell (x_c) is
729 plotted for *recN*$^{K35A/E473Q}$. Mean and standard deviation is shown (n = 50). (F) As (E) for
730 *recN*^{D472A}. (G) Density histogram of RecA filament lengths (*l*) across all time points of imaging
731 for wild type, *recN*^{D472A} and *recN*$^{K35A/E473Q}$ (n = 229). Distribution of *l* was found to be
732 significantly different between wild type and *recN*$^{K35A/E473Q}$ (p-value = 0.0005, 95% CI
733 [0.008051, 0.02846], Welch's t-test). Distribution of *l* was comparable between wild type and
734 *recN*^{D472A} (p-value = 0.1535, 95% CI [-0.003326, 0.02108]). All data shown are from pre-
735 divisional cells.

736

737 Supplementary content

738 Supplementary Results with detailed description of theory and quantitative analysis.
739 Supplementary figures (associated with main text).

740 Supplementary videos 1-6. Supplementary tables 1-3.

741

Figure 1

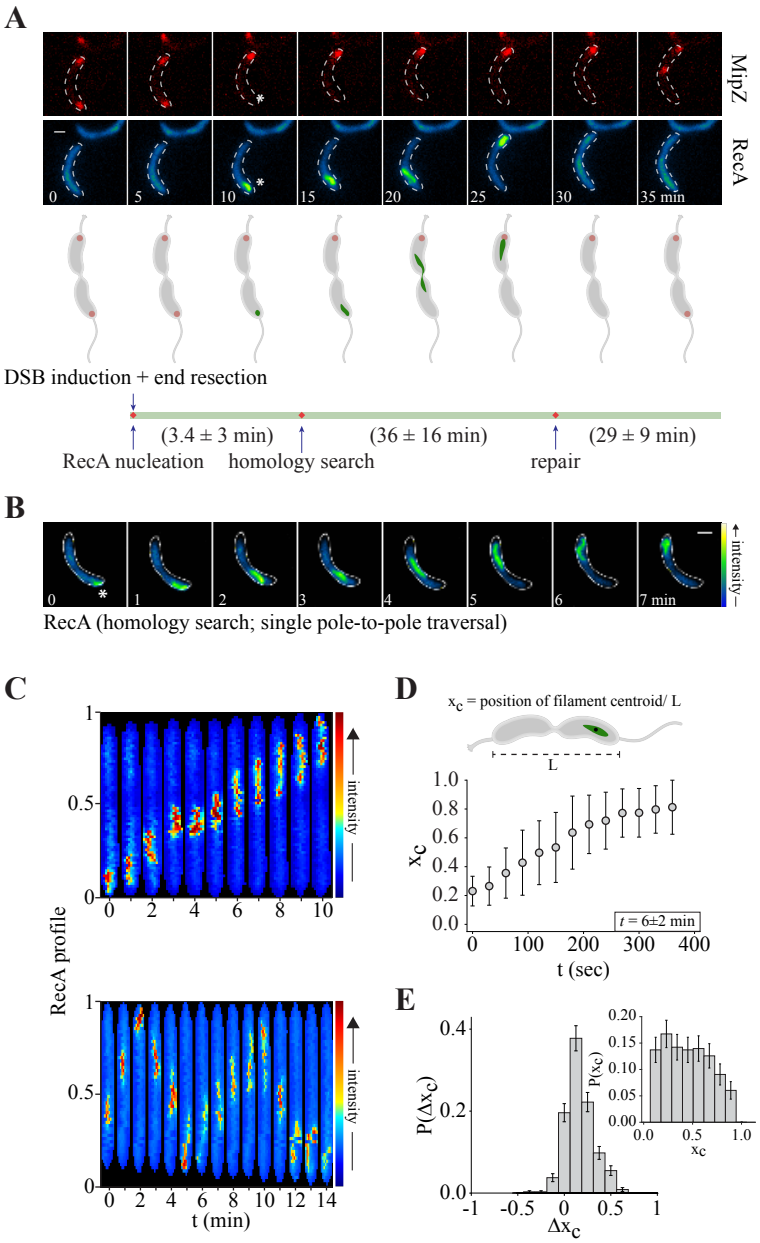
A
MipZ
RecA
0
5
10
15
20
25
30
35 min
DSB induction + end resection
(3.4 ± 3 min)
(36 ± 16 min)
(29 ± 9 min)
RecA nucleation
homology search
repair
B
0
1
2
3
4
5
6
7 min
intensity
RecA (homology search; single pole-to-pole traversal)
C
RecA profile
intensity
t (min)
D
x_c = position of filament centroid/ L
L
x_c
t (sec)
t = 6±2 min
E
$P(\Delta x_c)$
Δx_c
$P(x_c)$
x_c

Figure 2

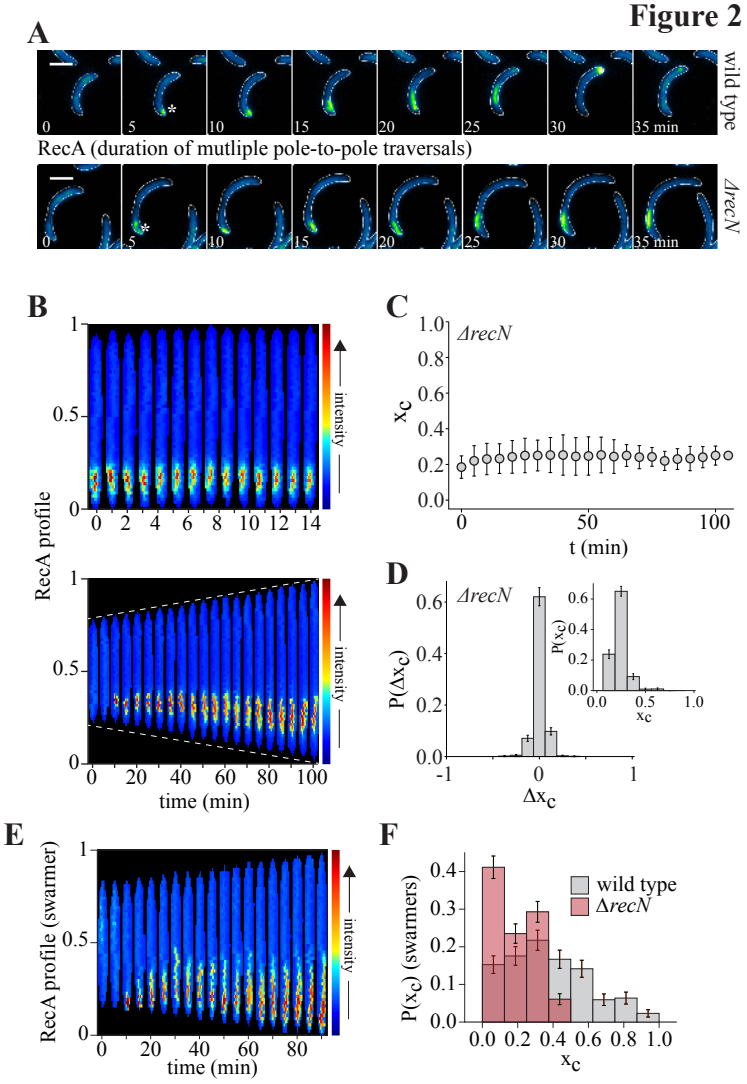
A
wild type
0
5
10
15
20
25
30
35 min
RecA (duration of mutliple pole-to-pole traversals)
ΔrecN
B
RecA profile
intensity
time (min)
C
ΔrecN
x_c
t (min)
D
ΔrecN
$P(\Delta x_c)$
Δx_c
$P(x_c)$
x_c
E
RecA profile (swarmer)
intensity
time (min)
F
wild type
ΔrecN
$P(x_c)$ (swarmers)
x_c

Figure 3

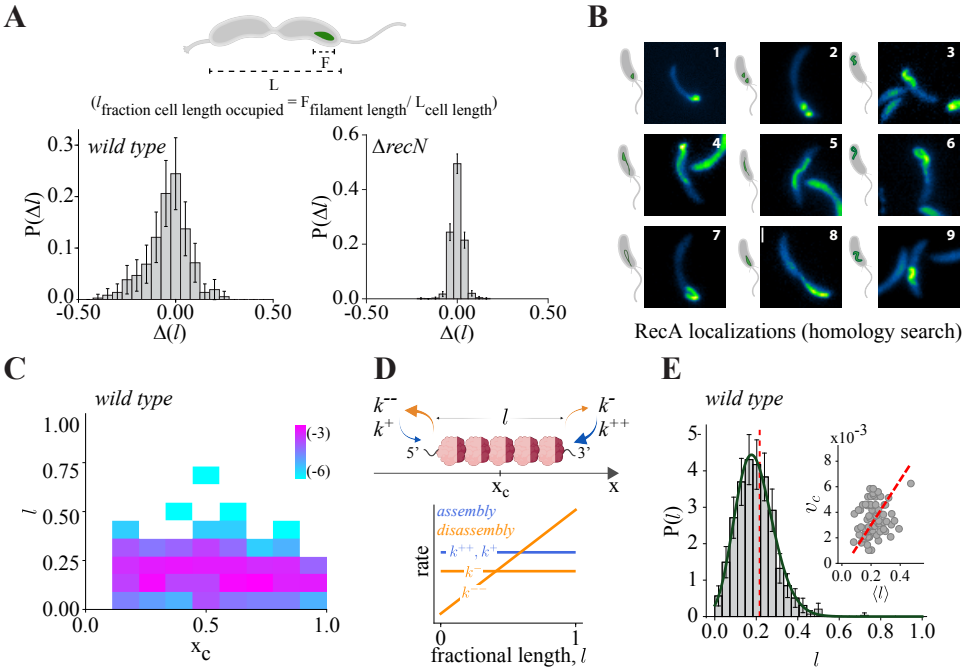
A
F
L
($l_{\text{fraction cell length occupied}} = F_{\text{filament length}} / L_{\text{cell length}}$)
wild type
ΔrecN
P(Δl)
Δ(l)
B
RecA localizations (homology search)
C
wild type
(-3)
(-6)
l
x_c
D
k--
k+
k-
k++
l
5'
3'
x_c
x
assembly
disassembly
rate
k++, k+
k-
k--
fractional length, l
E
wild type
P(l)
x10^-3
v_c
⟨l⟩
l

Figure 4

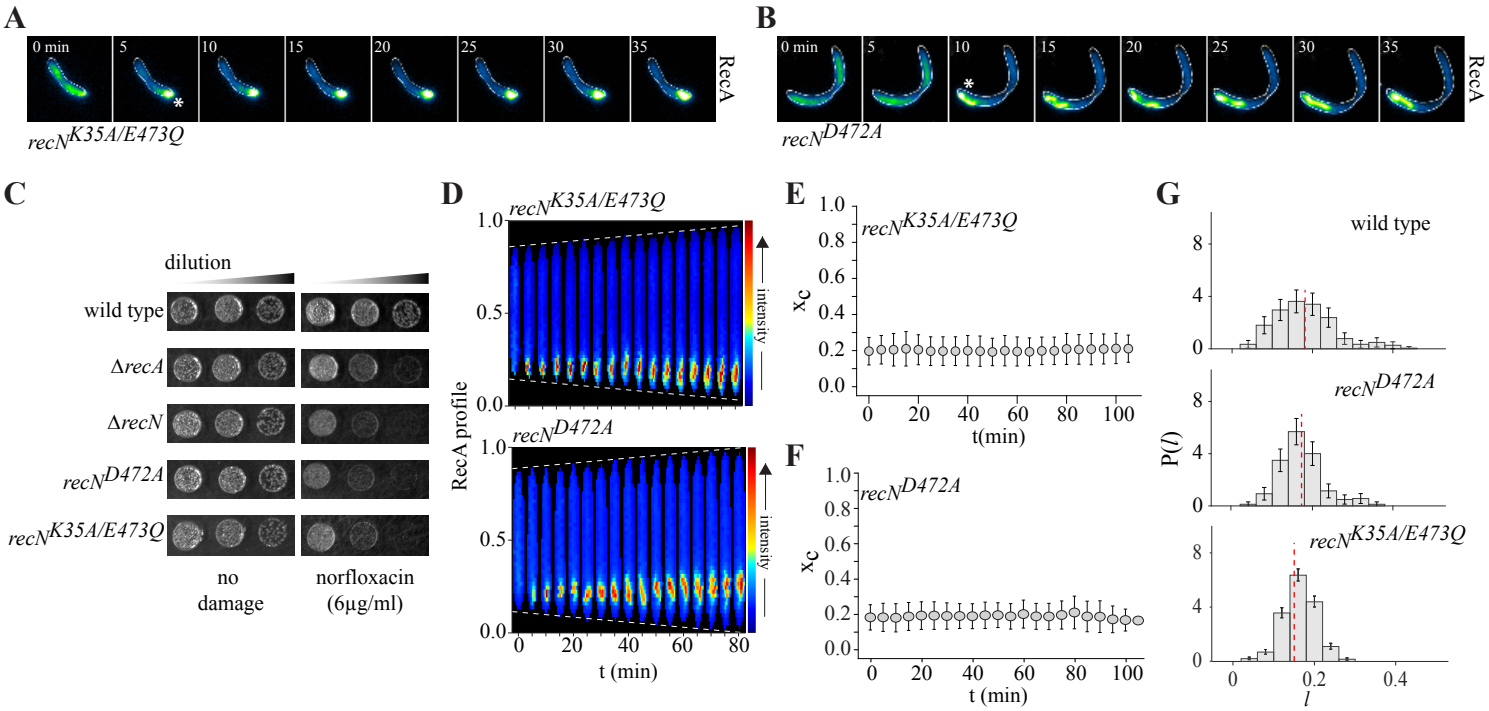
A
0 min
5
10
15
20
25
30
35
RecA
recNK35A/E473Q
B
0 min
5
10
15
20
25
30
35
RecA
recND472A
C
dilution
wild type
ΔrecA
ΔrecN
recND472A
recNK35A/E473Q
no damage
norfloxacin (6μg/ml)
D
recNK35A/E473Q
recND472A
RecA profile
intensity
t (min)
E
recNK35A/E473Q
xc
t(min)
F
recND472A
xc
t (min)
G
wild type
recND472A
recNK35A/E473Q
P(l)
l

Supplementary material

SMC protein RecN drives RecA filament translocation and remodelling for *in vivo* homology search

Afroze Chimthanawala, Jyotsana Parmar, Sujan Kumar, Krishnan S. Iyer, Madan Rao* and Anjana Badrinarayanan*

National Centre for Biological Sciences (TIFR), Bellary Road, Bangalore 560065, India

Contents:

Supplementary figures and figure legends (1-5)

Supplementary results (with associated figures 1-9)

Supplementary tables 1-3

Supplementary videos 1-6

Supplementary Figures:

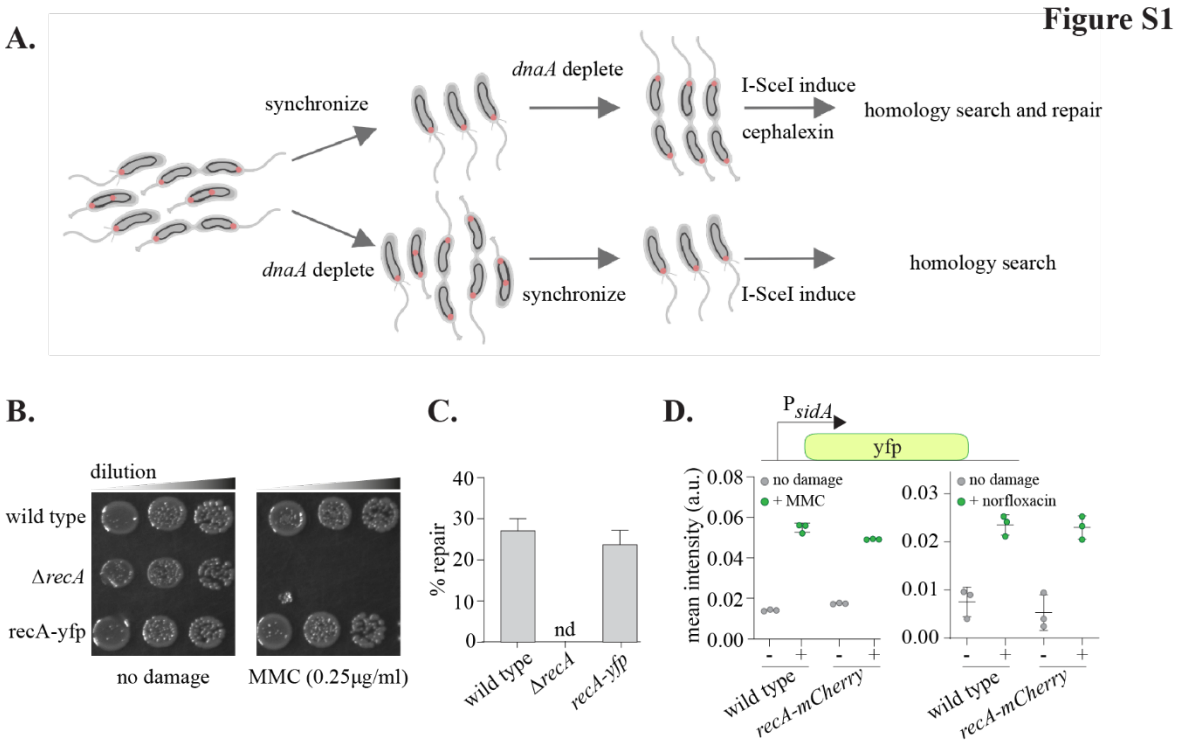

Fig. S1: Dynamics of RecA filament during homologous recombination. (A). Schematic of experimental setup. *Caulobacter* cells carrying either two completely replicated and segregated chromosomes or a single non-replicating chromosome (black circles inside the cell) are isolated as previously described. DSB site is integrated on the chromosome near the origin of replication and visualized via fluorescently-tagged MipZ (red dot), that forms foci at the polarly localized origin regions in *Caulobacter.* DSB is induced via regulated expression of a destabilized I-SceI enzyme. Cells with 2n chromosome content (pre-divisional cells) will carry out all steps of recombination (from homology search to repair) while cells with 1n chromosome content (swarmer cells) can be assessed for their ability to carry out homology search alone. **(B).** Strain expressing *recA-yfp* does not show increased sensitivity to generic DNA damaging agent, mitomycin-C (MMC), when compared with wild type cells (representative image from 3 independent repeats). **(C).** Repair events (reappearance of both MipZ localizations after loss of a single localization) are assessed across a 2 hr window of imaging for all cells that experienced a single DSB (as measured by loss of one but not both MipZ localizations). % cells showing repair is similar to previously published reports. No repair is detected (nd) in cells lacking *recA* (mean and standard deviation from three independent repeats (n= 100 cells for each repeat)) **(D).** RecA-YFP expressing cells are SOS proficient with similar induction levels as seen in the case of wild type cells. SOS induction levels are estimated by assessing the activity of the *sidA* promoter expressing a fluorophore.

Cells are treated with MMC or Norfloxacin for 2 hrs. Mean intensity is plotted for three independent repeats (n= 200 cells for each repeat).

Figure S2

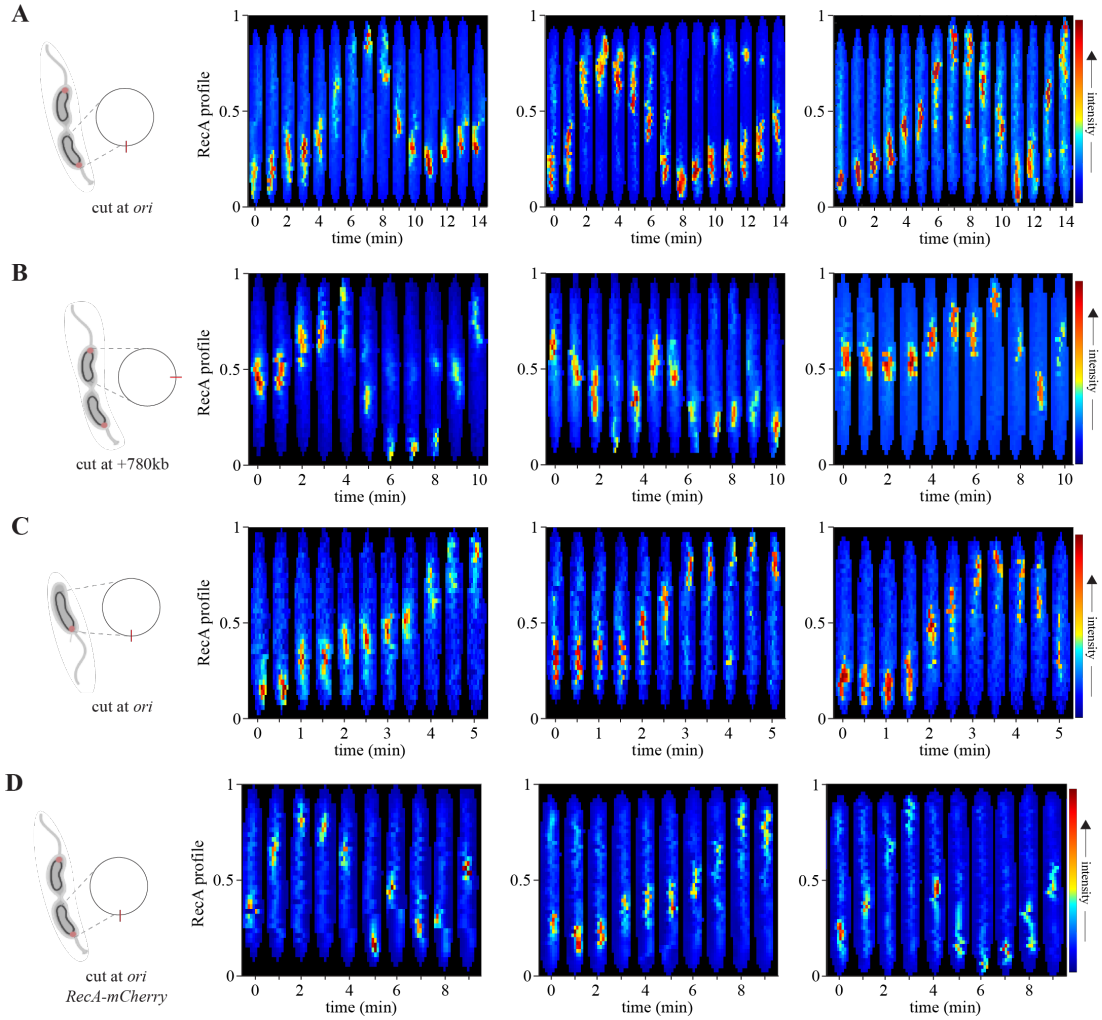

Fig. S2: Directional and dynamic movement of RecA filament during homology search. (A). Representative RecA-YFP fluorescence profiles across the length of the cell over pole-to-pole traversal events during homology search. DSB is induced near the origin of replication in non-replicating pre-divisional cells with two fully replicated and segregated copies of the chromosome. In all panels in this figure, *t0* is defined as the time point prior to the observation of a positive displacement of the RecA localization from the pole at which it first localized (DSB pole) **(B).** As (A) for DSB induced +780kb from the origin of replication. In this case, localization starts near ¼ or ½ position and proceeds towards either cell pole. **(C).** Representative RecA-YFP fluorescence profiles across the length of the cell over pole-to-pole traversal events during homology search. DSB is induced near the origin of replication in non-replicating swarmer cells with a single chromosome, thus lacking a homologous template for repair. **(D).** Representative RecA-mCherry fluorescence profile across the length of the cell show comparable dynamics to that observed in case of RecA-YFP in (A).

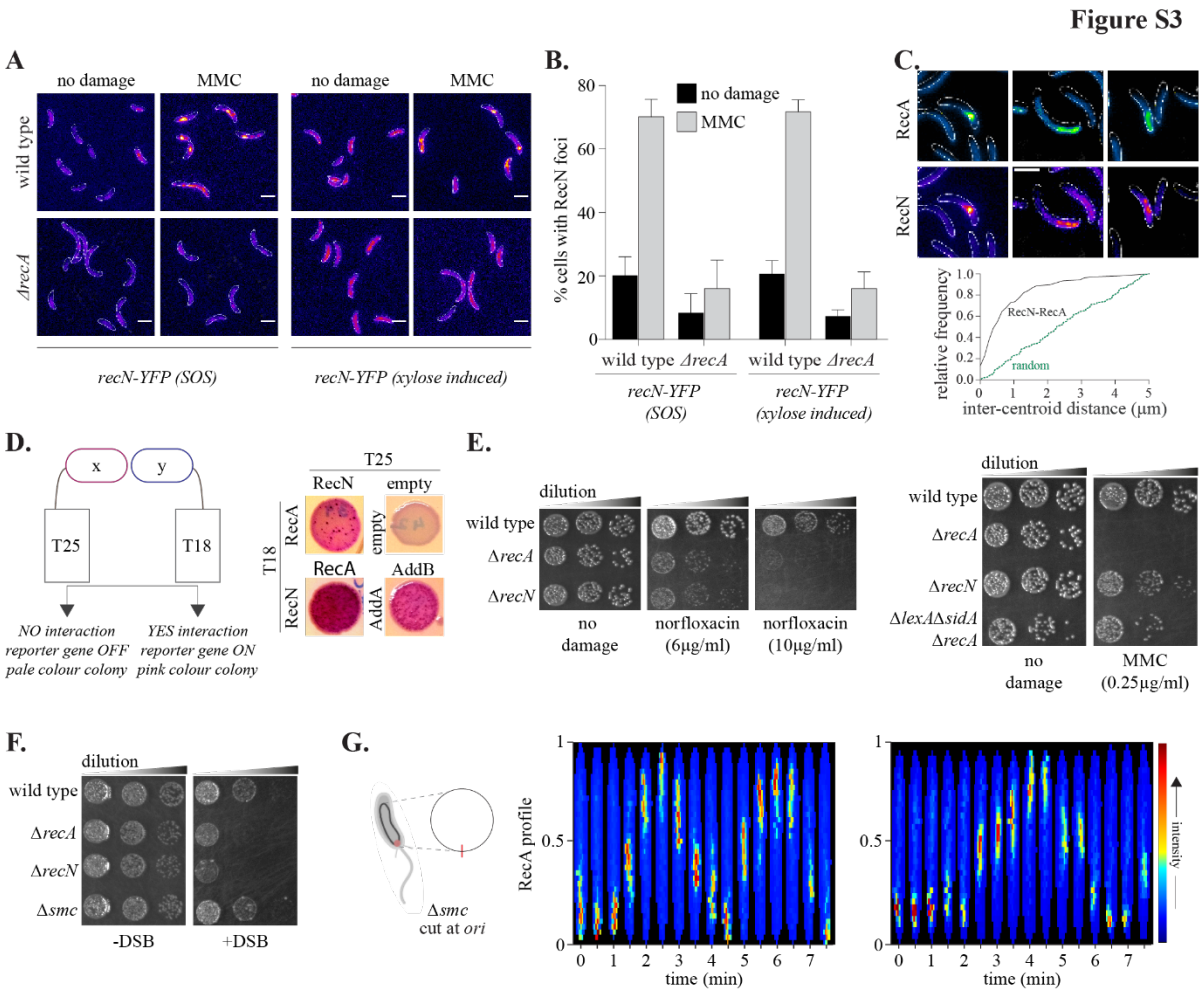

Fig. S3: RecN is essential for RecA filament movement *in vivo*. (A-B). RecN localization under DNA damage (MMC) is dependent on RecA. To distinguish between SOS induction requirement or RecA requirement, *recN* is also expressed from a xylose inducible promoter. In this case as well, localization in response to damage is dependent on presence of RecA (n = 100 cells for each condition, mean and standard deviation from three independent repeats). **(C).** RecA and RecN colocalize at a DSB. Representative images of RecA-mCherry and RecN-YFP are shown, after induction of a DSB at *ori.* Below, distance from centroid of RecN localization to centroid of RecA localization is measured (n = 100 localizations). As a control, distance from centroid of RecN to any pixel within the cell is plotted (random). **(D).** Physical interaction between RecN and RecA is assessed using the bacterial-two-hybrid assay. RecA/ RecN are fused to the T25 or T18 fragments of the adenylate cyclase gene. Positive interaction would bring the two fragments together and result in the expression of a reporter gene from a cAMP-inducible promoter, resulting in production of pink/ red colonies. Lack of interaction would result in pale colony colour. As a positive control AddA and AddB interaction is tested. *'empty'* refers to the T25 and T18 fragments alone. Representative image from at least three

independent repeats. **(E).** *ΔrecA* or *ΔrecN* cells are similarly sensitive to DSB-inducing agent norfloxacin. In case of MMC, which causes generic DNA damage, *ΔrecA* cells show higher sensitivity than *ΔrecN*. However, cells lacking *recA* with constitutive SOS response ON (*ΔlexAΔsidAΔrecA)* have similar sensitivity to MMC as *ΔrecN,* suggesting that both proteins are similarly required for MMC damage repair (excluding the function of RecA in regulating the SOS response). Representative image from at least three independent repeats. **(F).** *ΔrecA* or *ΔrecN* cells are similarly sensitive to DSB induction via I-SceI. In contrast, *Δsmc* cells show comparable growth to wild type cells. Representative image from at least three independent repeats. **(G).** Representative RecA-YFP fluorescence profiles across the length of the cell in cells lacking *smc.* Here, *t0* is defined as the time point prior to the observation of a positive displacement of the RecA localization from the pole at which it first localized (DSB pole).

Figure S4

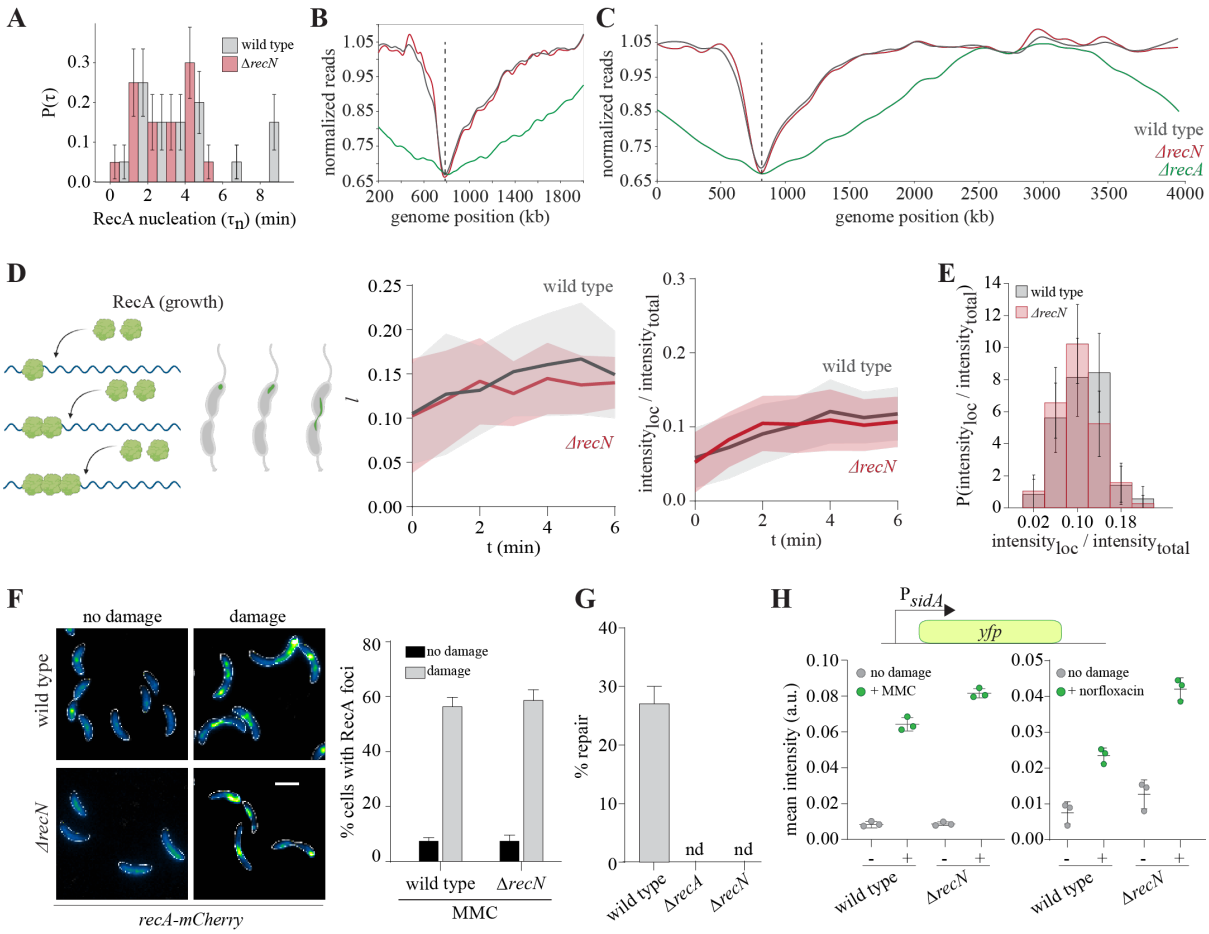

Fig. S4: RecN does not impact RecA nucleation (A). Probability distribution of RecA nucleation time (time between disappearance of a single MipZ marker *(t0)* and appearance of RecA localization at that position) for wild type (grey) and Δ*recN* (red) cells (n = 100). **(B).** Zoomed in (200−2000 kb) DSB processing profiles for cells induced with break at +780kb (dashed line) in wild type (grey), Δ*recN* (green) and Δ*recA* (red) cells. Sequencing reads are normalized to a no damage control and loss of reads around the break site is indicative of loss of double-stranded DNA. Cells lacking *recA* undergo 'rec-less' degradation, resulting in significant loss of sequencing reads around the DSB site. Representative plot from two independent repeats. **(C)** Whole genome profile for data in **(B)**. **(D).** RecA filament growth (time between RecA nucleation *(t0)* and start of first translocation cycle (in case of wild type)) is measured either as a function of change in RecA filament length (l) over time [right] or change in localization intensity over time (intensity_{loc} / intensity_{total}) [left] for wild type and *ΔrecN* cells. Solid line represents the mean and shaded region the standard deviation. **(E)** For reference, distribution of localization intensities for all cells is also shown (n=50). **(F).** RecA localization is dependent on DNA damage. Percentage cells with RecA localization with or

without MMC damage is plotted for wild type and *ΔrecN* cells (mean and standard deviation from three independent repeats, $n = 100$). **(G).** I-SceI-induced DSB repair events are estimated for wild type, *ΔrecA* and *ΔrecN* cells. Repair in absence of *ΔrecA* or *ΔrecN* is not detectable (nd) in a 2 hr window of imaging (n=100 cells for each repeat). Wild type and *ΔrecA* measurements are from Fig. S1C (mean and standard deviation from three independent repeats). **(H).** SOS induction levels are measured via P_{sidA}-yfp expression under MMC or Norfloxacin damage for wild type and *ΔrecN* cells (mean and standard deviation from three independent repeats (n=200 cells for each repeat)).

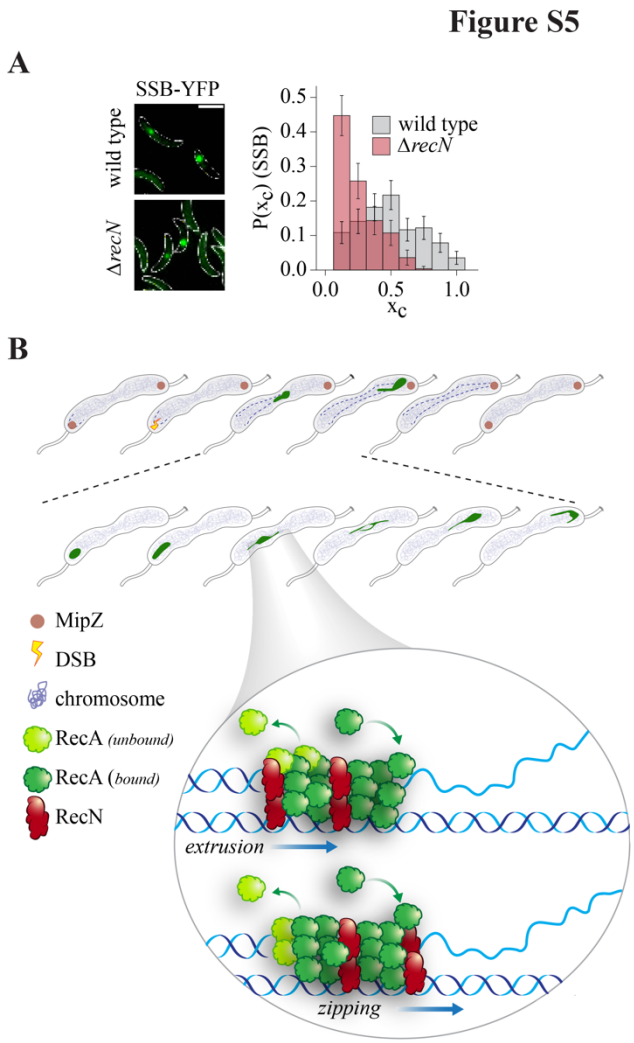

Fig. S5: Proposed mechanism for RecN-driven RecA filament translocation and remodeling during homology search. (A). [Above] Representative images of SSB-YFP localization upon induction of a single DSB in non-replicating swarmer cells. [Below] Probability distribution of SSB-YFP centroid position (x_c) in wild type (n = 369) and Δ*recN* cells (n = 278). **(B).** Proposed mechanism for RecN action on the RecA filament. Upon induction of a DSB near the polarly-localized origin, we observe localization of RecA to the break site. The RecA localization then dynamically translocates across the length of the cell undergoing several pole-to-pole traversal events before the homologous partner is found. This movement and associated remodeling of the nucleoprotein filament depends on RecN. We propose that RecN modulates RecA filament lengths during translocation via regulating rates of RecA subunit assembly-disassembly. In addition, RecN action on DNA (via possible bridging activity between ssDNA and dsDNA) can facilitate RecN-driven translocation of the RecA filament and its underlying DNA substrate. We use 'zipping' to refer to RecN action ahead of the filament and 'extrusion' for action behind the filament.

Supplementary Video Legends:

Video 1: RecA-YFP in pre-divisional cells after induction of a single DSB near the polar origin of replication. RecA-green; cell outline-white. Four individual cells shown. Time in min.

Video 2: RecA-YFP in swarmer cells after induction of a single DSB near the polar origin of replication. RecA-green; cell outline-white. Four individual cells shown. Time in min.

Video 3: RecA-YFP in pre-divisional cells lacking *recN,* after induction of a single DSB near the polar origin of replication. RecA-green; cell outline-white. Four individual cells shown. Time in min.

Video 4: RecA-YFP in swarmer cells lacking *recN,* after induction of a single DSB near the polar origin of replication. RecA-green; cell outline-white. Four individual cells shown. Time in min.

Video 5: RecA-YFP in pre-divisional cells carrying $recN^{D473A}$ mutant, after induction of a single DSB near the polar origin of replication. RecA-green; cell outline-white. Four individual cells shown. Time in min.

Video 6: RecA-YFP in pre-divisional cells carrying $recN^{K35A/E473Q}$ mutant, after induction of a single DSB near the polar origin of replication. RecA-green; cell outline-white. Four individual cells shown. Time in min.

Supplementary Results for

SMC protein RecN drives translocation and remodelling of RecA filament for homology search

Afroze Chimthanawala, Jyotsana Parmar, Sujan Kumar, Krishnan S. Iyer, Madan Rao and Anjana Badrinarayanan
National Centre for Biological Sciences (TIFR), Bellary Road, Bangalore 560065, India

CONTENTS

S1. Quantitative Analysis of experimental data 3

S2. Stochastic description of the RecN-assisted dynamics of the RecA filament 4
A. Mechanochemistry and Assembly-Disassembly Cycle 4
1. Mechanochemical states 4
2. Assembly-Disassembly Cycle 5
3. Reduction to an effective model 6
B. Dependence of assembly-disassembly rates on l 7
C. Stochastic Dynamics of the RecA-RecN filament 9

S3. Comparison with experiments : extracting fitting parameters 11
A. Wild type cells 11
B. $\triangle recN$ cells 13

References 14

S1. QUANTITATIVE ANALYSIS OF EXPERIMENTAL DATA

Images were analysed using Microbetracker/ Oufti [1, 2] and MatLab or manually assessed in ImageJ. In all cases, experiments were biologically replicated at least three times and pooled data from at least three independent repeats are plotted (after confirming reproducibility between replicates). Plots were generated using custom written code, MatLab (2019, 2020), R, Python or GraphPad Prism 8.0. Schematics were made using Biorender and Adobe Illustrator. Following image acquisition, phase contrast profiles of cells were segmented using Oufti. Mesh files were then overlayed on the raw images (.tiff). 'roipoly' function in Matlab was implemented to extract pixel values only within the desired cell ROI. Given the curved nature of Caulobacter cells, for the ease of analysis the ROIs of segmented cells were straightened. For this, firstly the ROI was rotated by angle equal to the angle between the major axis of the ROI and x-axis. This angle was estimated by extracting the image property 'Orientation' using MatLab function 'regionprops'. Secondly, a line was drawn across the cell length, positioned at mid-cell. This was taken as the reference line to which all pixels of the ROI were re-centered. Following this straightening, pixels were adjusted along the mid-cell line to maintain all cell information (cell area and fluorescence).

RecA nucleoprotein filament properties were analysed via two key dynamical variables - position of the centroid of RecA filament relative to the length of the cell (x_c) and length of the RecA filament relative to the cell length (l). In addition, intensity (i) was also estimated, as the ratio of RecA fluorescence within the localization to total cell fluorescence. To obtain the above-described parameters, an eCDF (Empirical Cumulative Distribution Function) plot was generated for the fluorescence intensities per pixel in every ROI throughout the time-lapse movie. From this, intensity value $\geq$ 96% of the eCDF plot was selected from a single frame as the threshold for automated detection of RecA nucleoprotein filament localizations, that allowed for accurate detections of most localizations in the movie. This threshold was then uniformly applied across for all frames of the time-lapse. Values below this threshold were considered as part of background fluorescence coming from the freely-diffusing pool of RecA-YFP and were not included for analysis of (x_c) or (l). RecA fluorescence profiles thus generated were visualized in the form of a kymograph generated in MatLab. Profiles were compared to the raw images obtained to ensure that false positive or false negative detections were avoided.

Δx_c and Δl were calculated by subtracting the value at the present frame from the value at the previous frame. To estimate velocity v_c, a least square fit of degree 1 was made for the x_c values during a traversal using 'polyfit' function in python. The slope of this linear fit was defined as the mean velocity of a traversal, v_c. The v_c values falling above or below the range 0.006 – 0.001 were considered as outliers, traversals with only 2 data points were excluded. These features were analyzed for cells during the 'homology search' phase as defined by the first recordable positive non-zero value for Δx_c, following the nucleation and growth of the RecA localization (Fig. S1A). The first time point $x_c(0)$ was set to the frame before the Δx_c value was non-zero. The last time point for a single traversal was recorded when the centroid of RecA localized at the opposite cell pole from where the mobility had started. We estimate that this phase represents a steady-state dynamic based on the following observations: a. distribution of l in invariant across time-points of imaging during the homology search phase (Fig. S1C-E). b. distribution of l is comparable between pre-divisional and swarmer cell states (where homology search is continuous, due to the inability to complete recombination-based repair) (Fig. S1B).

The nonlinear fits to the density histograms of (l) in the cases of wild type and *recN* deleted cells were generated using in-built functions in Mathematica. Using the respective histogram data, parameters in the equations (32) and (48) were estimated using the function "NonlinearModelFit" which uses the Levenberg-Marquardt algorithm. Reasonable initial conditions needed to be provided to the function/algorithm in order to ensure plausible estimates of the parameters. With these estimates, consistency checks for the probability density functions were done and the curves/graphs (green) plotted (Fig. S8-S9).

The > 95% confidence intervals to calculate Margin of Error (MoE) for probability distributions were estimated according to the formula for population proportion estimator,

$$\pi_k = P_k \pm z_{0.025}\sqrt{\frac{P_k(1-P_k)}{n}}$$

where n is the data/sample size, P_k is the empirical proportion calculated using the data for bin k, and π_k is the true population proportion for the bin k. To estimate the density, however, the above equation was divided by the respective bin widths δx_k.

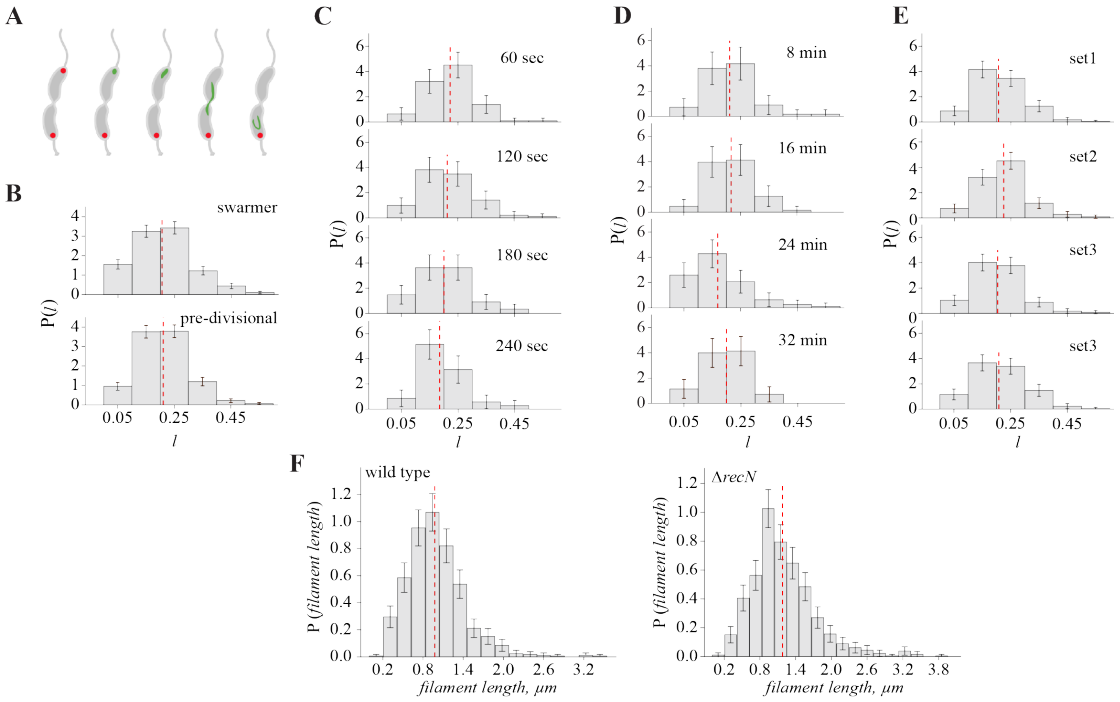

FIG. S1. A. Schematic depicting steps of RecA nucleation, growth and homology search. B. Density histogram of RecA filament lengths during homology search in swarmer and pre-divisional cells indicates that lengths are comparable ($n = 858$). C. Density histogram of RecA filament lengths at indicated time intervals during homology search indicates that lengths are comparable. Same set of cells are tracked across all time points ($n \geq 70$). D. Density histogram of RecA filament lengths during homology at indicated time windows of imaging indicates that lengths are comparable ($n \geq 70$). E. Density histogram of RecA filament lengths for subset of cells (25 cells in each set) from length distribution in Fig. 3E. F ($n \geq 214$). Density histogram of RecA filament lengths (in μm) for wild type ($n = 795$) or *recN* ($n = 852$) deletion mutants. Fraction length (l) is calculated from these values. In all plots, red dashed line is indicative of mean.

S2. STOCHASTIC DESCRIPTION OF THE RecN-ASSISTED DYNAMICS OF THE RecA FILAMENT

We provide a quantitative stochastic description of the mechanochemistry of RecN-assisted RecA filament dynamics.

A. Mechanochemistry and Assembly-Disassembly Cycle

1. *Mechanochemical states*

To do this, we first describe the conformation states of the RecA-RecN system, both unbound and bound to the DNA strand. RecA and RecN are both ATPases, and hence should exist in their native states and in their ATP-bound and ADP-bound states [3–7].

From [8–10] we know that RecA-ATP is bound to the ssDNA, while RecA-ADP is primed for unbinding from the DNA substrate. While there is no information yet on the DNA binding status of RecN-ATP or RecN-ADP, we do

know that a form of RecN binds to the DNA bound RecA-ATP [6]. Thus we will simply assume that there is, in addition to the native RecN, a bound state of RecN.

This is the conformation state space of the RecA-RecN system that we display in Fig. S2.

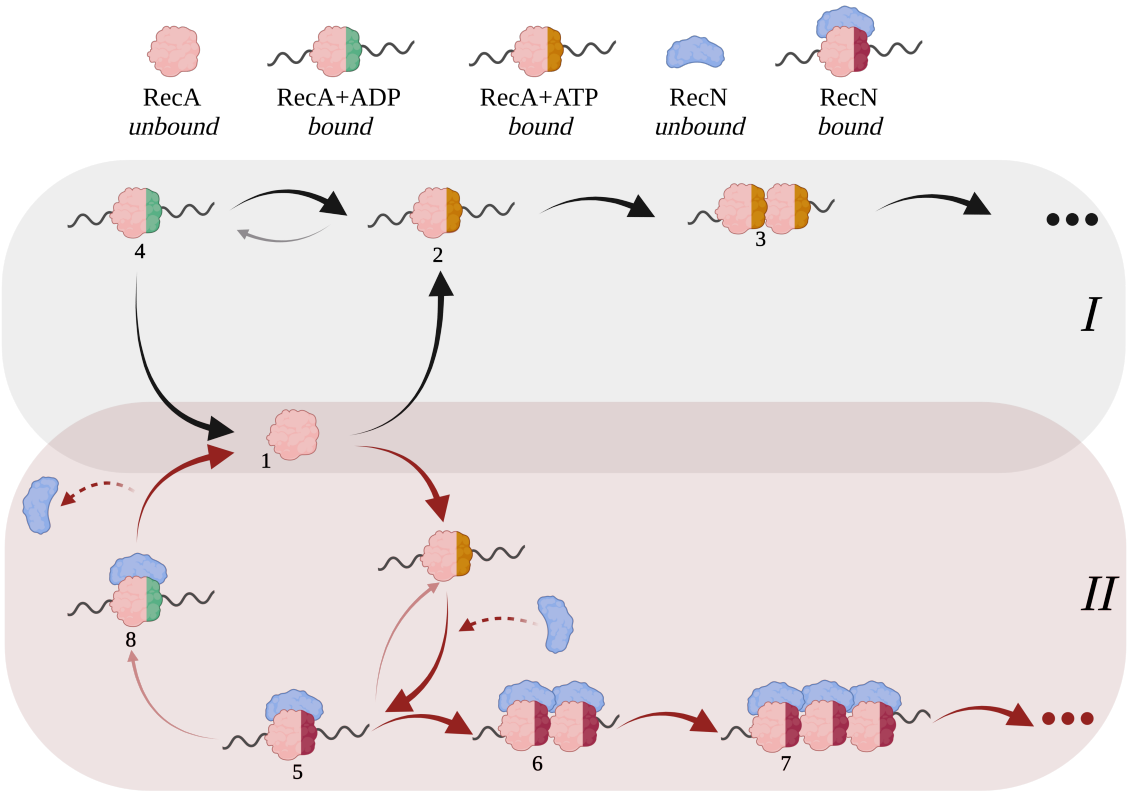

FIG. S2. (top) The conformation states of RecA and RecN, depend on their ATPase activity and their binding to the DNA substrate. (bottom) The assembly-disassembly network of RecA-RecN comprises two modules I and II, described in the text. Thick (thin) arrows denote higher (lower) rates. The directional bias in both the RecN-assisted RecA filament movement (in Module II), and RecA assembly in the recN mutant (Module I), is schematised here by a structural asymmetry of the bound states, which ultimately result in a left-right asymmetry in the binding-unbinding rates onto the DNA strand.

2. *Assembly-Disassembly Cycle*

We now describe the assembly-disassembly network of RecA and RecN on the DNA strand. This network comprises two strongly connected modules - Module I, which involves RecA alone, and Module II, which involves both RecA and RecN .

The Module I network is displayed in Fig. S3. Here the unbound RecA (node 1) can assemble on the DNA in the RecA-ATP bound state (node 2). From node 2, the RecA-ATP can either transform to RecA-ADP (node 4) by hydrolysis or can assemble an additional RecA-ATP to form a dimer (node 3). From node 3, the RecA-ATP dimer can either transform to node 5 by hydrolysis or can assemble an additional RecA-ATP to form a trimer (node 6), an so on (represented by •••). The polymerization happens unidirectionally along the DNA strand, from the $5'$ to the $3'$ end.

In Fig. S3, the thick black arrows denote transitions with higher rates, whereas the thin gray arrows denote transitions where the rates are low. It follows that in the absence of RecN, the RecA monomers can in principle be quickly assembled on the DNA substrate from the $5'$ to the $3'$ end to form a growing RecA filament.

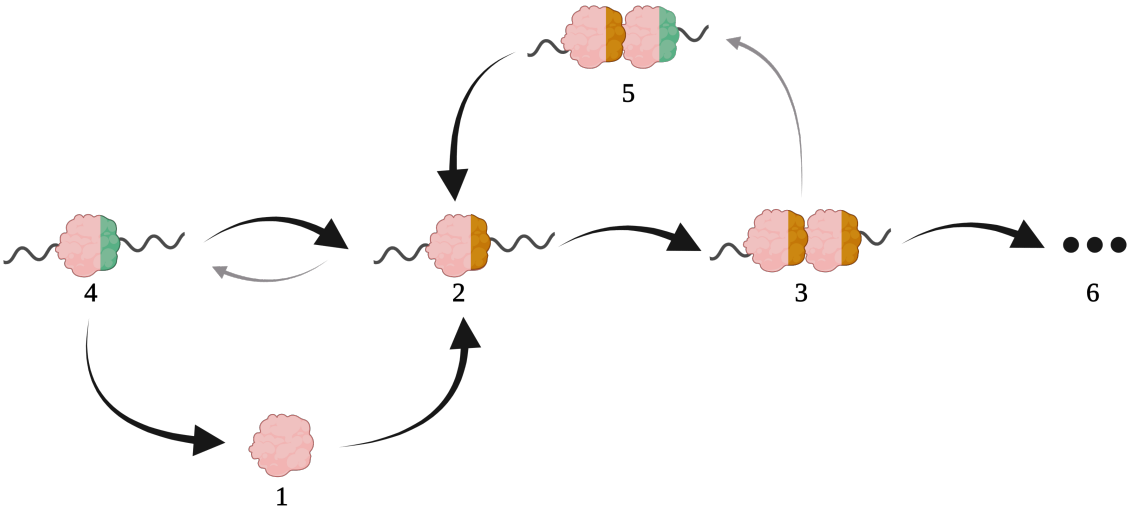

FIG. S3. Module I shows the assembly-disassembly network of RecA on DNA. The chemical reaction network comprises a set of nodes that transition from one to another via directed and weighted edges (arrows) that denote reaction paths. The darker arrows are associated with higher reaction rates.

Module II involves both RecA and RecN, and is shown in Fig. S4. Here the unbound RecA (node 1) can assemble on the DNA in the RecA-ATP bound state (node 2), which with the availability of unbound RecN gets transformed to a bound RecA-RecN complex (node 3). From node 3, the bound RecA-RecN complex can either hydrolyse to form RecA-ADP bound to RecN (node 6), followed by disassembly to node 1, or can assemble an additional RecA-RecN complex to form a dimer (node 4), and so on, ..., to form a filament of the RecA-RecN complex. As before, the thick red arrows denote higher transition rates, whereas the thin pink arrows denote transitions where the rates are low.

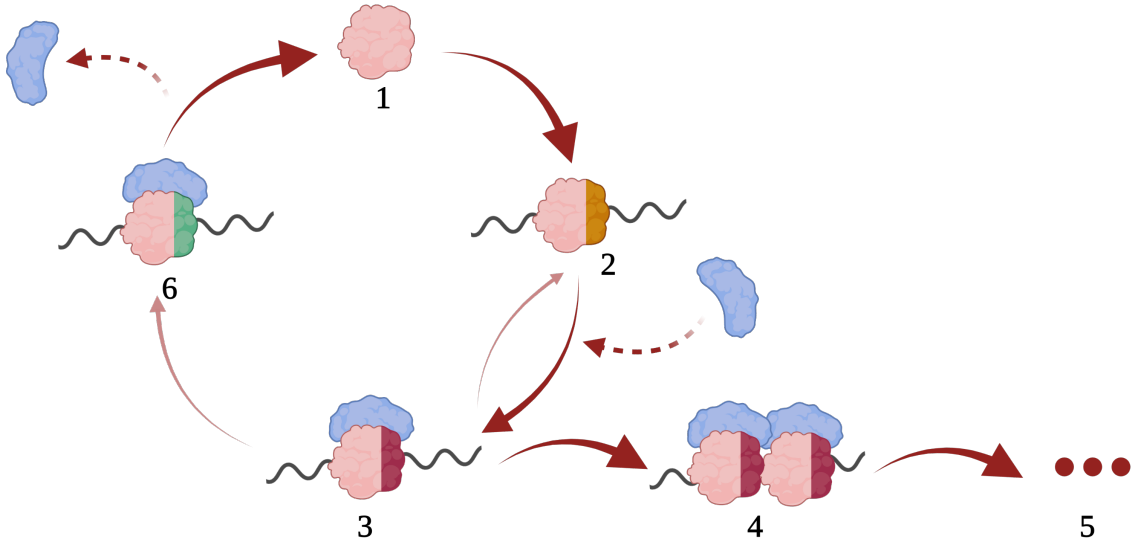

FIG. S4. Module II shows the assembly-disassembly network of RecA-RecN on DNA. The blue crescent protein represents unbound-RecN, which enters and leaves this module via the dashed arrows. Here again, the darker arrows are associated with higher reaction rates.

3. Reduction to an effective model

The full network depicted in Fig. S2, of which Modules I and II are a part, is complex and analytically intractable. We therefore need to come up with a suitable reduction of the network which has fewer nodes and directed edges,

while retaining the relevant features of the original. Here we present a systematic procedure to do so.

Our strategy is to prune those reactions in the network that do not contribute significantly to network output. Our method is based on a reaction flux analysis of stochastic chemical reaction networks [11–13], which monitors the intensity of the flow between chemical species over a given time interval. We then identify reactions that have low mean reaction flux, compared to a threshold, and eliminate the associated vertices and directed edges, together with modifying the edges in the reduced network. To implement this, we choose a node i and compute the signed vertex flux at that node, $F_i = \sum_{l_i} F_{i,l_i}$, where the sum is over all directed edges that enter or leave node i. If $F_i < F_{min}$, a threshold, the i-th node will be removed, except for the case where the i-th node represents a decisive reactant. All edges that were connected to at least one of the removed nodes will be removed, too. All other reactions are retained.

This coarse-graining strategy works best for a chemical network with a sequence of reactions that occur in series, with offshoots that are in parallel [11–13], which is precisely the network architecture displayed in Modules I and II.

Applying this procedure to the reaction network in Module I (Fig. S3), we see that node 4 has two strong arrows going away from it, and so the vertex flux of node 4 is very low. We thus prune this part of the network and introduce a directed edge from node 2 to node 1. Similarly node 5 can be eliminated, followed by introducing a directed edge from node 3 to node 2. This procedure can be carried out across the network. The rest of the nodes (and edges) such as 1, 2, 3, are retained. This leads to the reduced Module I shown in Fig. S5.

We prune Module II in the same way. Thus node 6 can be eliminated, whilst introducing a directed edge from node 3 to node 1. Likewise, node 2 can be eliminated, with the introduction of a strong directed edge from node 1 to node 3. The RecN that enters the reaction module with a dashed edge are decisive reactants and will be retained. These considerations lead to the reduced Module II shown in Fig. S5.

It is this reduced ladder model that is amenable to analytical treatment and will be investigated further. Before doing that, there are two comments that we would like to make regarding the reduced network. One, is that since RecA and RecN are ATPases, some of the directed edges in the network are driven by energy transduction and hence violate the condition of detailed balance. The second, is that both the systematic polymerisation of RecA in Module I and the RecA-RecN complex in Module II that is observed in the $\Delta recN$ and wild type cells, is unidirectional from the $5^{'}$ to $3^{'}$ on the DNA strand. This breaking of left-right symmetry (parity), must have a manifestation in a structural feature of both DNA-bound RecA, and DNA-bound RecA-RecN complex, that has been schematised in Figs. S3-S5.

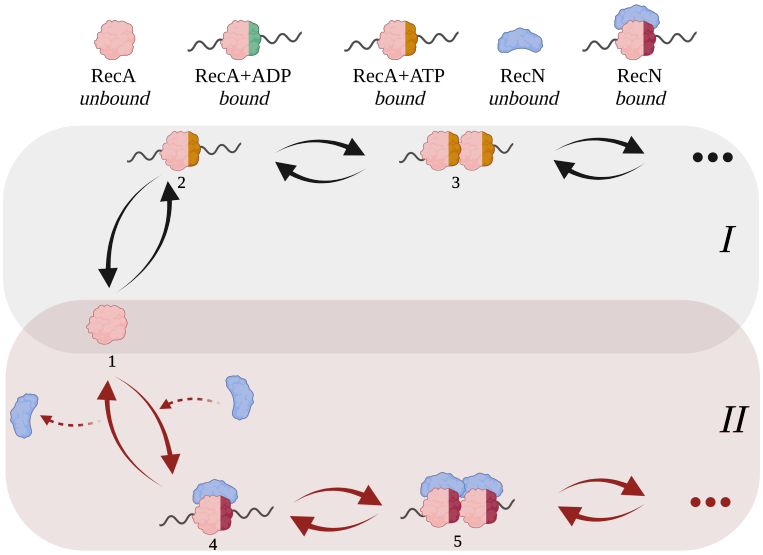

FIG. S5. Reduction of RecA-RecN assembly-disassembly following a Flux-based analysis. Here we prune the original network to reduce the number of vertices and directed edges without significantly changing the network flux.

B. Dependence of assembly-disassembly rates on l

To specify the reduced reaction network completely, we need to provide the assembly-disassembly rates associated with the directed edges. Ideally this should be obtained from independent experiments, such as FRAP, however this poses quite a challenge. Instead we extract some information about these microscopic rates from the experiments described in Figs. 1, 2 and 3 of the main manuscript.

We first note that the distribution of the centroid position x_c is uniform across the cell (Fig. 1E [inset]) and that the joint distribution $P(x_c, l)$ in Fig. 3C reveals that there are no "hot-spots". This would suggest that the dynamics of l does not depend on x_c. Further, the distribution of step sizes, both Δx_c and Δl show positive and negative values, suggesting that the dynamics of the filament proceeds via assembly and disassembly as it traverses across the cell (Fig. 1E and Fig. 3A).

The most important aspect of the experimental data is that the distribution of filament length $P(l)$ at steady state shows a peak at a finite value of $l = l^*$, a value that is significantly smaller that the cell length in both the wild type and the $\Delta recN$ cells (also the filament never extends over the cell length). This we argue, implies that the rates of assembly and disassembly cannot be constant. For, if the assembly rate is larger than the disassembly rate, then the filament will grow without limit. With the same token, if the disassembly rate is larger than the assembly rate, then the filament will shrink to zero. The dynamical flows corresponding to these scenarios is shown in Fig. S6 (i), (ii). The constant assembly-disassembly rates cannot be made to balance each other robustly at a particular length and will not give rise to the observed finite peak l^* at steady state.

This implies that the assembly-disassembly rates must depend on the length of the filament. Clearly, to obtain a peaked distribution at l^*, one should arrange that assembly exceeds disassembly at $l < l^*$, and disassembly exceeds assembly at $l > l^*$. Such a *negative feedback* between the assembly-disassembly rates and the filament length Fig. S6 (iii), (v), provides a homeostatic balance leading to a finite mean filament length with small fluctuations about it. This results in a stable fixed point at $l = l^*$ in the flow diagram Fig. S6 (iii), (iv).

It is clear that if the feedback is positive, then the filament will either show unbridled growth or complete shrinkage resulting in an unstable fixed point l^*.

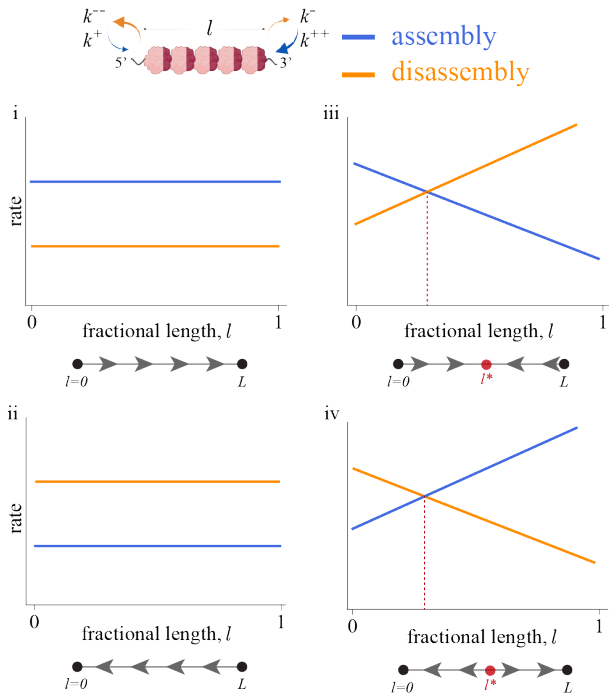

FIG. S6. Homeostatic balance of RecA filament length arising from RecN-influenced assembly-disassembly of RecA units on the DNA strand. In order to obtain a fixed mean filament length by assembly-disassembly, the rates have to be dependent on the length l. The corresponding flow diagrams are shown below each panel.

Two final observations from the experiments: (i) The RecA filament appears to always nucleate from the DSB site, and does not seem to nucleate elsewhere on the DNA strand. This suggests that the nucleation is strongly heterogeneous. (ii) Since the filament integrity is maintained, i.e., the filament does not exhibit any breaks during its traversal across the cell, we assume that the RecA-RecN assembles/disassembles only at the two ends of the filament and not in the interior.

C. Stochastic Dynamics of the RecA-RecN filament

As discussed in the main text, our observation that the RecN-assisted movement of the RecA filament is strongly correlated with the stochastic remodelling of its length, immediately suggests that the RecN ATPase drives the RecA filament both by its motor activity via extrusion and the assembly-disassembly rates of RecA units on the DNA strand. Here we describe a stochastic kinetic model that integrates both the RecN-assisted DNA mobility and the dynamics of RecN influenced assembly-disassembly of the RecA units on the DNA strand using the effective reaction network described above.

We describe the stochastic dynamics of nucleation, growth and movement of the filament using a kinetic approach. If the movement arises from a combination of motor-assisted movement and assembly-disassembly processes, it is then appropriate to describe the RecA dynamics in the lab frame, taking into account both the movement of the DNA strand and the movement of the RecA filament on the DNA strand (Fig. S7).

Nucleation occurs at the DSB site, with a binding rate k^+. As more RecA units are added, it grows into a RecA-filament with a left end x_l and right end x_r. As a result of the stochastic assembly-disassembly processes, the ends x_l and x_r move to the left or right with specific rates.

We denote by k^- the bare rate of unbinding of the RecA-RecN complex. Initially, we expect $k^+ > k^-$, for the RecA-RecN to form a nascent filament post nucleation. Subsequently, since the filament integrity is maintained, we will assume that the RecA-RecN assembles/disassembles only at the two ends, x_l and x_r, of the filament Fig. S7. To account for the RecN-induced unidirectional movement of the filament in the wild type cells, we allow for a different assembly rate at the right, k^{++}, and a disassembly rate at the left, k^{--}.

Mathematically, the pure motor-driven extrusion limit corresponds to a perfect correlation between k^{++} and k^{--} processes. For simplicity, we will use the language of assembly-disassembly processes, but it should be borne in mind that the stochastic dynamics encompasses *both* motor-assisted movement and assembly-disassembly and their combinations.

Since we are concerned with the dynamics of the filament well away from the cell poles, we have assumed that the cell boundaries do not affect the dynamics of x_l and x_r.

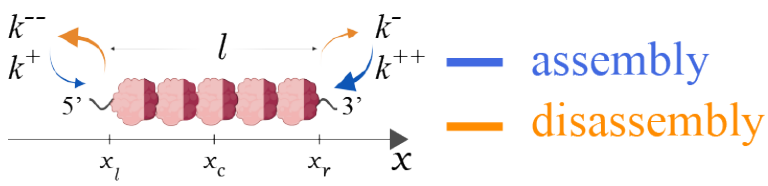

FIG. S7. The RecN-assisted RecA filement dynamics relative to the lab frame (x-axis) is a combination of motor-assisted movement and assembly-disassembly.

Every time a RecA-RecN monomer is added or removed from the right end, x_r moves to the right or left by an amount σ (similarly for the left end x_l). The right and left ends of the RecA-RecN filament thus move as a biased random walker with a stochastic dynamics given by the Langevin equation,

$$\frac{1}{\sigma}\frac{d\mathrm{x}_r}{dt} = \left(k^{++}(l) - k^{-}(l)\right) + \sqrt{2\left(k^{++}(l) + k^{-}(l)\right)}\,\xi_r(t) \tag{1}$$

$$\frac{1}{\sigma}\frac{d\mathrm{x}_l}{dt} = \left(k^{--}(l) - k^{+}(l)\right) + \sqrt{2\left(k^{--}(l) + k^{+}(l)\right)}\,\xi_l(t) \tag{2}$$

which comprises a drift term

$$F_r(l) = k^{++}(l) - k^{-}(l) \tag{3}$$

$$F_l(l) = k^{--}(l) - k^{+}(l) \tag{4}$$

and a diffusive term,

$$G_r(l) = \sqrt{2(k^{++}(l) + k^{-}(l))} \tag{5}$$

$$G_l(l) = \sqrt{2(k^{--}(l) + k^{+}(l))} \tag{6}$$

that multiplies the noises $\xi_r(t)$ and $\xi_l(t)$. The noise is taken to be a Gaussian white noise with zero mean and unit variance. We may rewrite Eq. 1,2 in terms of the the centroid and filament length, $\mathrm{x}_c = \frac{\mathrm{x}_r + \mathrm{x}_l}{2}$ and $l = \mathrm{x}_r - \mathrm{x}_l$,

respectively,

$$\frac{1}{\sigma}\frac{d\mathrm{x}_c}{dt} = F_c(l) + \frac{1}{2}G_r(l)\ \xi_r(t) + \frac{1}{2}G_l(l)\ \xi_l(t) \tag{7}$$

$$\frac{1}{\sigma}\frac{dl}{dt} = F_l(l) + G_r(l)\ \xi_r(t) - G_l(l)\ \xi_l(t) \tag{8}$$

where

$$F_c(l) = \frac{\Big(k^{++}(l) - k^{-}(l)\Big) + \Big(k^{--}(l) - k^{+}(l)\Big)}{2} \tag{9}$$

$$F_l(l) = \Big(k^{++}(l) + k^{+}(l)\Big) - \Big(k^{--}(l) + k^{-}(l)\Big) \tag{10}$$

We will henceforth remember to measure x_c and l in units of σ, and so they will now be considered dimensionless. We note two features of the above equations -

1. Eq. 7 for the centroid x_c is a function of l and noise alone.
2. Eq. 8 for the length l is independent of x_c.

Since the rates and hence G_r, G_l are dependent on the stochastic variable l, the noise is *multiplicative*, and hence special care needs to be taken to interpret the stochastic equation [15]. We will choose the Stratonovich interpretation.

These observations imply that one can obtain an expression for the mean centroid velocity $\mathrm{v}_c \equiv \langle \dot{\mathrm{x}_c} \rangle$, by simply averaging Eq. 7 over all noise realisations,

$$\mathrm{v}_c = \Big\langle F_c(l) \Big\rangle + \frac{1}{2}\Big\langle G_r(l)\xi_r(t) \Big\rangle + \frac{1}{2}\Big\langle G_l(l)\xi_l(t) \Big\rangle \tag{11}$$

The last two averages on the right side of the above equation are nonzero due to the Stratonovich interpretation. To evaluate these, we make use of Novikov's theorem for gaussian noise ξ with zero mean, which takes the form [18],

$$\Big\langle G\left[y\left(\xi(t)\right)\right]\xi(t) \Big\rangle = \int \left\langle \frac{\delta G}{\delta \xi(t')} \right\rangle \Big\langle \xi(t')\xi(t) \Big\rangle\ dt' \tag{12}$$

For a noise ξ with unit variance,

$$\Big\langle G\left[y\left(\xi(t)\right)\right]\xi(t) \Big\rangle = \left\langle \frac{\delta G}{\delta \xi(t)} \right\rangle \tag{13}$$

Using Novikov's theorem, we obtain

$$\frac{1}{2}\Big\langle G_{r,l}(l)\xi_{r,l}(t) \Big\rangle = \frac{1}{2}\left\langle \frac{\delta G_{r,l}(l)}{\delta \xi_{r,l}(t)} \right\rangle \tag{14}$$

$$= \frac{1}{2}\left\langle \frac{\delta G_{r,l}(l)}{\delta l(t)}\ \frac{\delta l(t)}{\delta \xi_{r,l}(t)} \right\rangle \tag{15}$$

by the chain rule. The response function, $\delta l(t)/\delta \xi_{r,l}(t)$, is calculated from Eq. 8, using the Stratonovich interpretation,

$$\frac{\delta l(t)}{\delta \xi_r(t)} = \frac{1}{2}\,G_r(l) \tag{16}$$

$$\frac{\delta l(t)}{\delta \xi_l(t)} = -\frac{1}{2}\,G_l(l) \tag{17}$$

These results from Novikov's theorem allow us to evaluate the averages in Eq. 11, to obtain,

$$\mathrm{v}_c = \langle F_c(l) \rangle + \frac{1}{4}\langle G_r'(l)G_r(l) \rangle - \frac{1}{4}\langle G_l'(l)G_l(l) \rangle \tag{18}$$

where prime denotes a derivative with respect to l. To evaluate these moments, for prescribed functions $F_c(l)$ and $G_{r,l}(l)$, we need to obtain the marginal distribution $P(l,t)$. This can be obtained by constructing a Fokker-Planck equation for Eq. 8.

To do this, we first rewrite Eq. 8 as,

$$\frac{dl}{dt} = F_l(l) + \sqrt{G_r^2(l) + G_l^2(l)}\ \xi(t) \tag{19}$$

where $\xi(t) = \xi_r(t) + \xi_l(t)$. The associated Fokker-Planck equation [15, 17] in the Stratonovich interpretation (ref) is,

$$\frac{\partial P(l,t)}{\partial t} = -\frac{\partial}{\partial l}\Big[F_l(l)P(l,t)\Big] + \frac{1}{2}\frac{\partial}{\partial l}\Big[\sqrt{G_r^2 + G_l^2}\ \frac{\partial}{\partial l}\sqrt{G_r^2 + G_l^2}\ P(l,t)\Big] \tag{20}$$

which is of the form,

$$\frac{\partial P(l,t)}{\partial t} = -\frac{\partial}{\partial l}\, J_l \tag{21}$$

We will be interested in the stationary solution of Eq. 20 at steady state, i.e., when $\partial P(l,t)/\partial t = 0$. Further, since l is bounded, the probability current $J_l = 0$, i.e.,

$$-\frac{2F_l(l)}{\sqrt{G_r^2 + G_l^2}}P(l) + \frac{\partial}{\partial l}\Big[\sqrt{G_r^2 + G_l^2}\ P(l,t)\Big] = 0 \tag{22}$$

The solution obtained by straightforward integration is,

$$P(l) = \frac{N}{\sqrt{G_r^2 + G_l^2}}\exp\Big[\int_0^l \frac{2F_l(l^{'})}{G_r^2 + G_l^2}dl^{'}\Big] \tag{23}$$

where N is obtained from the normalization condition,

$$\int_0^\infty P(l)dl = 1 \tag{24}$$

Eqs. 18 and 23 together with the normalization condition, are the main results of this section. To compare with the experimental observations in wild type and $\Delta recN$ cells, we need to provide the functional forms of F_l and $G_{r,l}$.

But before doing that, we can make some general comments. From Eq. 10, we see that F_l is the net imbalance between assembly and diassembly, and so l will grow if $F_l > 0$, will shrink if $F_l < 0$, and a balance is met when $F_l = 0$. To obtain a distribution that is peaked at a finite l, one must have $F(l) > 0$ at small l (assembly dominates disassembly) and $F_l < 0$ at large l (disassembly dominates assembly). The steady state distribution $P(l)$ will then peak at l^*, given by the balance condition $F_l = 0$. This distribution will typically be skewed about its peak value.

S3. COMPARISON WITH EXPERIMENTS : EXTRACTING FITTING PARAMETERS

A. Wild type cells

Following the discussion in Sect. S2 B, we take the RecN-dependent disassembly rate k^{--} at the left end of the filament to be linearly dependent on l and all other rates to be constant, i.e.,

$$k^{--} = k_1 l + k_2 \tag{25}$$

This implies that for large l, disassembly exceeds assembly and provides a mechanism for homeostatic balance at a finite fixed point l^*.

Such negative feedback control by RecN could be direct, via influence of RecN on RecA turnover within the filament or indirect via modulation of the underlying DNA substrate [6, 7, 22]. This could drive RecA turnover at opposite ends of the filament [3, 5, 20, 21].

Using this form in Eqs. 5, 6, 4 we get,

$$G_r^2 + G_l^2 = 2(k^{++} + k^{+} + k^{-} + k_2 + k_1 l) \equiv 2(a + k_1 l) \tag{26}$$

$$F_l = (k^{++} + k^{+} - k^{-} - k_2 - k_1 l) \equiv A - k_1 l \tag{27}$$

With these forms, the steady state distribution (Eq. 23) is,

$$P(l) = \frac{N}{\sqrt{2(a+k_1 l)}} \exp\Big[\int_0^l \frac{A - k_1 l'}{a + k_1 l'} dl'\Big] \tag{28}$$

$$= \frac{N}{\sqrt{2} a^{c+1/2}} (a + k_1 l)^c e^{-l} \tag{29}$$

where,

$$c = \frac{A+a}{k_1} - \frac{1}{2} = \frac{2(k^{++}+k^{+})}{k_1} - \frac{1}{2} \tag{30}$$

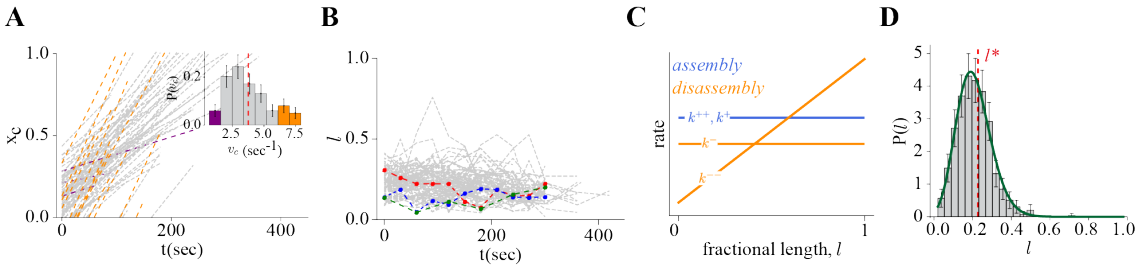

FIG. S8. (A) Centroid position x_c versus time for each wild type cell at steady state. The centroid positions are fit to straight lines using a least-squares fit, from which we extract (inset) the distribution of the centroid velocity P (v_c), which is sharply peaked at (v_c) = 0.004 ± 0.002. The purple and orange data are outliers. (B) Fractional filament length l for each wild type cell versus time at steady state. The coloured dots and lines denote representative time series for l. (C) The disassembly rate (k^{--}) is taken to be length dependent while the assembly rates (k^{++}, k^{+}) are constant. (D) Fitting the experimental data (gray histogram) with the theory Eq. 32 (green). Red dashed vertical line is the mean length l^*.

At this stage we comment on some robust qualitative features of the derived distribution $P(l)$, which are readily apparent in the observed wild type distribution. skewness, $\langle l \rangle$(mean l for a single traversal)$> l^*$, linearity for small l, exponential decay for large l,

We determine N from the normalization condition, Eq. 24, giving

$$N = \frac{\sqrt{2}\, a^{c+1/2}}{\Gamma(1+c, a)} k_1^{-c} e^{-a/k_1} \tag{31}$$

where the argument of the incomplete Γ function, $c+1>0$, and the normalised distribution, (recall that l is in units of σ),

$$P(l) = \frac{e^{-a/k_1}(a/k_1)^c}{\Gamma(1+c, a)} \left(1 + \frac{k_1}{a} l\right)^c e^{-l} \tag{32}$$

The qualitative features of the observed wild type distribution, namely (i) $P(l \to 0) > 0$, (ii) $P(l)$ is linear in l for small l, (iii) $P(l)$ is a skewed distribution about the peak, (iv) The peak value of l is less than the mean, i.e., $l^* < \langle l \rangle$ and (v) $P(l)$ falls off exponentially for larger l, are features of the distribution Eq. 32.

We find that the normalized form of (Eq. 32), fits the observed wild type distribution perfectly (Fig. S8), with fit parameters, the prefactor

$$\frac{e^{-a/k_1}(a/k_1)^c}{\Gamma(1+c, a)} = 0.307672 \tag{33}$$

$$k_1/a = 3.80084 \tag{34}$$

$$c = 23.8146 \tag{35}$$

(Note that the experimental distribution in Fig. S8D is plotted with the fractional length relative to the cell size, l/L. Taking this into account introduces another fit parameter in the exponential term in Eq. 32, which we determine to be $d = 54.1388$.) That is 3 independent parameters, k_1, a, c, which can be written in terms of the 5 original kinetic parameters $k^{+}, k^{-}, k^{++}, k_1, k_2$, implying there is a lot of degeneracy in the values of these kinetic parameters. This

would suggest that the distribution is robust to slight cell-to-cell variations in these kinetic parameters. We verify this robustness by pooling the WT data sets into batches of 25 cells, and comparing their respective distributions (Fig. S1E).

Having determined $P(l)$, we can now unpack the relation Eq. 18 between the mean centroid velocity v_c and the moments of $P(l)$. Using Eqs. 9, 5, 6, we see that

$$F_c(l) = \frac{1}{2}\left(k^{++} + k_2 - k^- - k^+ + k_1 l\right) \equiv \frac{1}{2}(B + k_1 l) \tag{36}$$

$$G_r = \sqrt{2\left(k^{++} + k^-\right)} \tag{37}$$

$$G_r' = 0 \tag{38}$$

$$G_l(l) = \sqrt{2(k^+ + k_2 + k_1 l)} \tag{39}$$

$$G_l'(l) = \frac{k_1}{\sqrt{2(k^+ + k_2 + k_1 l)}} \tag{40}$$

Thus,

$$\mathrm{v}_c = \frac{1}{2}\left(B - \frac{k_1}{2} + k_1 \langle l \rangle\right) \tag{41}$$

i.e., a linear relation between the mean centroid velocity and the mean filament length. This remarkable relation is verified in Fig. 3E [inset] in the main manuscript. We note that this graph in Fig. 3E, allows us to estimate a microscopic rate k_1, the feedback associated with the length dependent disassembly rate. We also find that the intercept is negative, which gives a bound

$$\left(k^{++} + k_2 - k^- - k^+\right) < \frac{k_1}{2} \tag{42}$$

for the microscopic rates.

B. $\triangle$*recN* cells

Following the discussion in Sect. S2 B for the mutant $\triangle recN$ cells, we take the disassembly and assembly rates k^-, k^{++} at the right end of the filament to be length l dependent and of the form,

$$k^- = m_2 + m_1 l^2 \tag{43}$$

$$k^{++} = k_2 + k_1 l \tag{44}$$

and all other rates to be constant. Here again for large l, disassembly exceeds assembly, leading to homeostatic balance at a finite fixed point l^*.

A possible molecular mechanism for such negative feedback control could be due to strain-dependent dissociation of RecA molecules at large filament lengths [23]. Indeed, evidence for cooperative/ allosteric loading of RecA has also been reported previously [4, 21, 23].

Using this form in Eqs. 5, 6, 4 we get,

$$G_r^2 + G_l^2 = 2(k_2 + k_1 l + k^+ + m_2 + m_1 l^2 + k^{--}) \equiv 2(a + k_1 l + m_1 l^2) \tag{45}$$

$$F_l = k_2 + k_1 l + k^+ - m_2 - m_1 l^2 - k^{--} \equiv A + k_1 l - m_1 l^2 \tag{46}$$

With these forms, the steady state distribution (Eq. 23) is,

$$P(l) \propto \frac{1}{\sqrt{2(a + k_1 l + m_1 l^2)}} \exp\left[\int_0^l \frac{A + k_1 l' - m_1 l'^2}{a + k_1 l' + m_1 l'^2} dl'\right] \tag{47}$$

$$\propto \left(a + k_1 l + m_1 l^2\right)^c \exp\left[\mu \tan^{-1}\left(\frac{2m_1 l + k_1}{d}\right)\right] e^{-l} \tag{48}$$

where, the parameters are known functions of the rates.

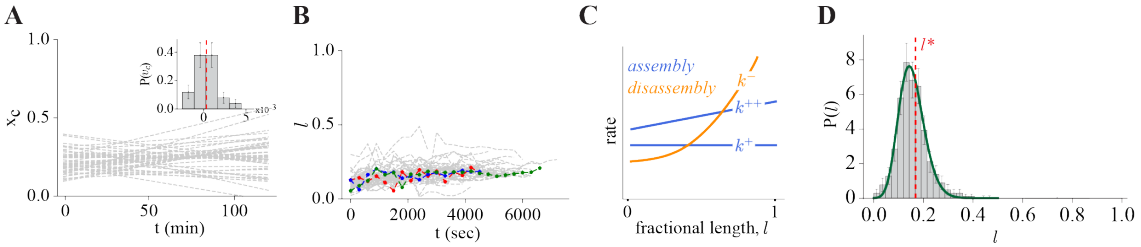

FIG. S9. (A) Centroid position x_c versus time for each wild type cell at steady state. The centroid positions are fit to straight lines using a least-squares fit, from which we extract (inset) the distribution of the centroid velocity P (v_c), which is sharply peaked at (v_c) = 0.0004 ± 0.00005. The purple and orange data are outliers. (B) Fractional filament length l for each wild type cell versus time at steady state. The coloured dots and lines denote representative time series for l. (C) The assembly rate ($k^{++} = -k_1 l^2 + k_2$) is taken to be length dependent while the disassembly rates (k^{--}, k^{-}) are constant. (D) Fitting the experimental data (gray histogram) with the theory curve (green). Red dashed vertical line denotes the mean length l^*.

We find that the distribution Eq. 48, when normalised numerically, fits the observed $\triangle recN$ distribution perfectly (Fig. S9D), with normalisation constant, $A = 5.3453$, the rest of the parameters

$$a = 0.657841 \tag{49}$$
$$k_1 = 7.66902 \tag{50}$$
$$m_1 = 0.0181797 \tag{51}$$
$$c = 21.0296 \tag{52}$$
$$d = 24.2558 \tag{53}$$
$$\mu = 5.46204 \tag{54}$$

and the parameter that enters the exponential term $\delta = 91.9232$ (since distribution is plotted in terms of the fractional length).

If we assume upfront that in $\triangle recN$ cells, left end of the growing filament does not change from its initial position, then the stochastic dynamics of the filament only involves the Langevin equation for x_r, Eq. 1. The filament length $l = x_r$, while the centroid position $x_c = \frac{x_r}{2}$ changes only because of the filament elongation.

[1] A. Paintdakhi, B. Parry, M. Campos, I. Irnov, J. Elf, I. Surovtsev, C. Jacobs-Wagner, Oufti: an integrated software package for high-accuracy, high-throughput quantitative microscopy analysis. Mol Microbiol. 99, 767–777 (2016).
[2] O. Sliusarenko, J. Heinritz, T. Emonet, C. Jacobs-Wagner, High-throughput, subpixel precision analysis of bacterial morphogenesis and intracellular spatio-temporal dynamics. Mol. Microbiol. 80, 612–627 (2011).
[3] Joo, S. A. McKinney, M. Nakamura, I. Rasnik, S. Myong, T. Ha, Real-Time Observation of RecA Filament Dynamics with Single Monomer Resolution. Cell. 126, 515–527 (2006).
[4] J. C. Bell, S. C. Kowalczykowski, RecA: Regulation and Mechanism of a Molecular Search Engine. Trends in Biochemical Sciences. 41, 491–507 (2016).
[5] J. M. Cox, O. V. Tsodikov, M. M. Cox, Organized Unidirectional Waves of ATP Hydrolysis within a RecA Filament. PLoS Biol. 3, e52 (2005).
[6] L. A. Uranga, E. D. Reyes, P. L. Patidar, L. N. Redman, S. L. Lusetti, The cohesin-like RecN protein stimulates RecA-mediated recombinational repair of DNA double-strand breaks. Nat Commun. 8, 15282 (2017).
[7] E. D. Reyes, P. L. Patidar, L. A. Uranga, A. S. Bortoletto, S. L. Lusetti, RecN Is a Cohesin-like Protein That Stimulates Intermolecular DNA Interactions in Vitro. Journal of Biological Chemistry. 285, 16521–16529 (2010).
[8] S. C. Kowalczykowski, Biochemistry of genetic recombination: energetics and mechanism of DNA strand exchange. Annu Rev Biophys Biophys Chem. 20, 539–575 (1991).
[9] S. H. Kim, K. Ragunathan, J. Park, C. Joo, D. Kim, T. Ha, Cooperative conformational transitions keep RecA filament active during ATPase cycle. J Am Chem Soc. 136, 14796–14800 (2014).
[10] S. H. Kim, T. Ahn, T. J. Cui, S. Chauhan, J. Sung, C. Joo, D. Kim, RecA filament maintains structural integrity using ATP-driven internal dynamics. Sci Adv. 3, e1700676 (2017).
[11] J. Proppe and M. Reiher, Mechanism Deduction from Noisy Chemical Reaction Networks, J. Chemical Theory and Computation **15**, 357-370 (2018).
[12] K. Han, W.H. Green and R.H. West, On-the-fly pruning for rate-based reaction mechanism generation, Computers & Chemical Engineering **100**, 1-8 (2017).
[13] G. Liu, M. T. Swihart and S. Neelamegham, Sensitivity, principal component and flux analysis applied to signal transduction: the case of epidermal growth factor mediated signaling, Bioinformatics **21**, 1194-1202 (2005).

[14] L. Mohapatra, B. L. Goode, P. Jelenkovic, R. Phillips, and J. Kondev. Design Principles of Length Control of Cytoskeletal Structures. Ann. Rev. Biophys. 45, 85-116 (2016).
[15] N. G. van Kampen, Ito versus Stratonovich, J. Stat. Phys. **24**, 175–187 (1981).
[16] C. W. Gardiner, Handbook of Stochastic Methods (2nd edition), Springer (1985), esp. after eq. (6.4.11).
[17] A. Baule, K.V. Kumar, S. Ramaswamy, Exact solution of a Brownian inchworm model for self-propulsion, J. Stat. Mech. **11**, 11008 (2008).
[18] E. A. Novikov, Soviet Physics — JETP 20, 1290 (1965).
[19] H. Risken, The Fokker-Planck Equation: Methods of Solution and Applications (Springer, Berlin, 1996).
[20] Q. Shan, J. M. Bork, B. L. Webb, R. B. Inman, M. M. Cox, RecA protein filaments: end-dependent dissociation from ssDNA and stabilization by RecO and RecR proteins. J Mol Biol. 265, 519–540 (1997).
[21] J. C. Bell, J. L. Plank, C. C. Dombrowski, S. C. Kowalczykowski, Direct imaging of RecA nucleation and growth on single molecules of SSB-coated ssDNA. Nature. 491, 274–278 (2012).
[22] K. Keyamura, T. Hishida, Topological DNA-binding of structural maintenance of chromosomes-like RecN promotes DNA double-strand break repair in Escherichia coli. Commun Biol. 2, 413 (2019).
[23] G. V. Shivashankar, M. Feingold, O. Krichevsky, A. Libchaber, RecA polymerization on double-stranded DNA by using single-molecule manipulation: the role of ATP hydrolysis. Proc Natl Acad Sci U S A. 96, 7916–7921 (1999).

Supplementary table 1: Strains used in present study

Strain name	Genotype	Strain construction/ source
CB15N	NA1000	
NABC439	CB15N; *ΔrecN::gent*^{R}	([1])
NABC2	CB15N; *ΔrecA*	([2])
NABC443	CB15N; *ΔrecA::gent*^{R}	NABC2 was transformed with pNABC496 followed by pNABC482 to link *recA* deletion with *gent*^{R}.
NABC444	CB15N; *ΔrecA::kan*^{R}	NABC2 was transformed with pNABC496 followed by pNABC497 to link *recA* deletion with *kan*^{R}.
NABC445	CB15N; P_{xyl}-*recA-mCherry::spec*^{R}	CB15N was transformed with pNABC484 plasmid to integrate *recA-mCherry* linked to *spec*^{R} at the P_{xyl} locus.
NABC446	CB15N; P_{xyl}-*recA-mCherry::gent*^{R}	CB15N was transformed with pNABC481 plasmid to integrate *recA-mCherry* linked to *gent*^{R} at the P_{xyl} locus.
NABC447	CB15N; P_{xyl}-*recA-YFP::gent*^{R}	CB15N was transformed with pNABC487 plasmid to integrate *recA-YFP* linked to *gent*^{R} at the P_{xyl} locus.
NABC448	CB15N; P_{xyl}-*recA-YFP::spec*^{R}	CB15N was transformed with pNABC480 plasmid to integrate *recA-YFP* linked to *spec*^{R} at the P_{xyl} locus.
NABC449	CB15N; *recN-YFP::spec*^{R}	CB15N was transformed with pNABC489 plasmid to integrate *recN-YFP* linked to *spec*^{R} at the endogenous locus through two-step recombination procedure ([3]).
NABC450	CB15N; *mipZ-mCherry::kan*^{R}	CB15N was transformed with pNABC485 plasmid to integrate *mipZ-mCherry* linked to *kan*^{R} at the endogenous locus.
NABC451	CB15N; *mipZ-mCherry::gent*^{R}	CB15N was transformed with pNABC486 plasmid to integrate *mipZ-mCherry* linked to *gent*^{R} at the endogenous locus.
NABC452	CB15N; *recN(D472A)::specR*	CB15N was transformed with pNABC490 plasmid to generate a specific mutation in the ATP binding domain of RecN through two- step recombination procedure. The resultant strain was transformed with pNABC488 to link *recN(D472A)* with *spec*^{R}.
NABC453	CB15N; *recN(E473Q)::specR*	CB15N was transformed with pNABC491 plasmid to generate a specific mutation in the ATP hydrolysis domain of RecN through two-step recombination procedure. The resultant strain was transformed with pNABC488 to link *recN(E473Q)* with *spec*^{R}.
NABC454	CB15N; pMT687-P_{sidA}-*YFP::kan*^{R}	CB15N was transformed with pNABC498 plasmid.

NABC455	CB15N; P_{xyl}-*recA-mCherry::gent*^{R}; pMT687-P_{sidA}-*YFP::kan*^{R}	NABC446 was transformed with pNABC498 plasmid.
NABC456	CB15N; *ΔrecA::gentR*; *recN-YFP::spec*^{R}	NABC449 was transduced with lysate of a strain harboring *recA* deletion (NABC443) and selected for *gent*^{R} that is linked to deletion.
NABC457	CB15N; ΔrecN::*gent*^{R}; P_{xyl}-*recN-YFP::spec*^{R}	NABC439 was transformed with pNABC483 plasmid to integrate *recN-YFP* linked to *spec*^{R} at the P_{xyl} locus.
NABC458	CB15N; ΔrecN::*gent*^{R}; P_{xyl}-*recN-YFP::spec*^{R}; *ΔrecA::kan*^{R}	NABC457 was transduced with lysate of a strain harboring *recA* deletion (NABC444) and selected for *kan*^{R} that is linked to deletion.
NABC459	CB15N; Δ*recN::gent*^{R}; pMT687-P_{sidA}-*YFP::kan*^{R}	NABC439 was transformed with pNABC498 plasmid.
NABC460	CB15N; P_{xyl}-*recA-mCherry::spec*^{R}; *ΔrecN::gent*^{R}	NABC445 was transduced with lysate of a strain harboring *recN* deletion (NABC439) and selected for *gent*^{R} that is linked to deletion.
NABC413	P_{lacI}-*lacI(hfa locus)*; P_{lac}-*dnaA(dnaA locus)*	([1])
NABC461	P_{lacI}-*lacI(hfa locus)*; P_{lac}-*dnaA(dnaA locus);* I-SceI site(after CCNA_00029)::*tet*^{R}; P_{van}-*I-SceI::chlor*^{R}	([4])
NABC462	P_{lacI}-*lacI(hfa locus)*; P_{lac}-*dnaA(dnaA locus);* I-SceI site(after CCNA_00029)::*tet*^{R}; P_{van}-*I-SceI::chlor*^{R}; *ΔrecA::gent*^{R}	NABC461 was transduced with lysate of a strain harboring *recA* deletion (NABC443) and selected for *gent*^{R} that is linked to deletion.
NABC463	P_{lacI}-*lacI(hfa locus)*; P_{lac}-*dnaA(dnaA locus);* I-SceI site(after CCNA_00029)::*tet*^{R}; P_{van}-*I-SceI::chlor*^{R}; *ΔrecN::gent*^{R}	NABC461 was transduced with lysate of a strain harboring *recN* deletion (NABC439) and selected for *gent*^{R} that is linked to deletion.
NABC464	P_{lacI}-*lacI(hfa locus)*; P_{lac}-*dnaA(dnaA locus);* I-SceI site(after CCNA_00029)::*tet*^{R}; P_{van}-*I-SceI::chlor*^{R}; *Δsmc::kan*^{R}	NABC461 was transduced with lysate of a strain harboring *smc* deletion (Tung B. K. Le, 2013) and selected for *kan*^{R} that is linked to deletion.
NABC465	P_{lacI}-*lacI(hfa locus)*; P_{lac}-*dnaA(dnaA locus);* I-SceI site(after CCNA_00029)::*tet*^{R}; P_{van}-*I-SceI::chlor*^{R}; *mipZ-YFP::kan*^{R}	([4])
NABC466	P_{lacI}-*lacI(hfa locus)*; P_{lac}-*dnaA(dnaA locus);* I-SceI site(after CCNA_00029)::*tet*^{R}; P_{van}-*I-SceI::chlor*^{R}; *mipZ-YFP::kan*^{R}; *ΔrecA::gent*^{R}	([4])
NABC467	P_{lacI}-*lacI(hfa locus)*; P_{lac}-*dnaA(dnaA locus);* I-SceI site(after CCNA_00029)::*tet*^{R}; P_{van}-*I-SceI::chlor*^{R}; *mipZ-mCherry::kan*^{R}; P_{xyl}-*recA-YFP::gent*^{R}	NABC461 was transduced with lysate of a strain harboring *mipZ-mCherry* linked to *kan*^{R} (NABC450) integrated at endogenous locus. Resultant strain was transduced with lysate ofa strain harboring *recA-YFP* linked to *gent*^{R} (NABC447) integrated at the P_{xyl} locus.

NABC468	P_{lacI}-*lacI(hfa locus)*; P_{lac}-*dnaA(dnaA locus);* I-SceI site(after CCNA_00029)::*tet*^{R}; P_{van}-*I-SceI::chlor*^{R}; *mipZ-mCherry::kan*^{R}; P_{xyl}-*recA-YFP::spec*^{R}; *ΔrecN::gent*^{R}	NABC461 was transduced with lysate of a strain harboring *mipZ-mCherry* linked to *kan*^{R}(NABC450) integrated at endogenous locus. Resultant strain was transduced with lysate ofa strain harboring *recA-YFP* linked to *spec*^{R} (NABC448) integrated at the P_{xyl} locus. Finally, lysate of NABC439 was transduced togenerate a *recN* deletion linked to *gent*^{R}.
NABC469	P_{lacI}-*lacI(hfa locus)*; P_{lac}-*dnaA(dnaA locus);* I-SceI site(after CCNA_00029)::*tet*^{R}; P_{van}-*I-SceI::chlor*^{R}; *mipZ-mCherry::kan*^{R}; P_{xyl}-*recA-YFP::gent*^{R}; *recN(D472A)::spec*^{R}	NABC467 was transduced with lysate of a strain harboring *recN(D472A)* linked to *spec*^{R} (NABC452).
NABC470	P_{lacI}-*lacI(hfa locus)*; P_{lac}-*dnaA(dnaA locus);* I-SceI site(after CCNA_00029)::*tet*^{R}; P_{van}-*I-SceI::chlor*^{R}; *mipZ-mCherry::kan*^{R}; P_{xyl}-*recA-YFP::gent*^{R}; *recN(E473Q)::spec*^{R}	NABC467 was transduced with lysate of astrain harboring *recN(E473Q)* linked to *spec*^{R} (NABC453).
NABC471	P_{lacI}-*lacI(hfa locus)*; P_{lac}-*dnaA(dnaA locus);* I-SceI site(after CCNA_00727)::*tet*^{R}	NABC413 was transformed with a pNPTS138 vector ([5]) to integrate *I-SceI* site after CCNA_00727 through two-step recombination procedure.
NABC472	P_{lacI}-*lacI(hfa locus)*; P_{lac}-*dnaA(dnaA locus);* I-SceI site(after CCNA_00727)::*tet*^{R}; parSpMT1site (after CCNA_00747)::*spec*^{R}; P_{van}-*I-SceI::chlor*^{R}	([5])
NABC473	P_{lacI}-*lacI(hfa locus)*; P_{lac}-*dnaA(dnaA locus);* I-SceI site(after CCNA_00727)::*tet*^{R}; P_{van}-*I-SceI::chlor*^{R}; parSpMT1site (after CCNA_00747)::*spec*^{R}; *ΔrecA::gent*^{R}	([5])
NABC474	P_{lacI}-*lacI(hfa locus)*; P_{lac}-*dnaA(dnaA locus);* I-SceI site(after CCNA_00727)::*tet*^{R}; P_{van}-*I-SceI::chlor*^{R}; parSpMT1site (after CCNA_00747)::*spec*^{R}; *ΔrecN::gent*^{R}	NABC472 was transduced with lysate of a strain harboring *recN* deletion (NABC439) and selected for *gent*^{R} that is linked to deletion.
NABC475	P_{lacI}-*lacI(hfa locus)*; P_{lac}-*dnaA(dnaA locus);* I-SceI site(after CCNA_00727)::*tet*^{R}; P_{van}-*I-SceI::chlor*^{R}; P_{xyl}-*recA-YFP::spec*^{R}	NABC471 was transduced with lysate of a strain harboring I-SceI enzyme (NABC472) linked to *chlor*^{R} integrated at the P_{van} locus. The resultant strain was transduced with lysateof a strain harboring *recA-YFP* (NABC448) linked to *spec*^{R} integrated at the P_{xyl} locus.

NABC476	BTH101; pKT25; pUT18C	([5])
NABC477	BTH101; pKT25-*addB::kan*^{R}; pUT18C-*addA::carb*^{R}	([6])
NABC478	BTH101; pKT25-*recA::kan*^{R}; pUT18C-*recN::carb*^{R}	BTH101 was co-transformed with pNABC494 ([6]) and pNABC493 for the bacterial-two-hybrid assay.
NABC479	BTH101; pKT25-*recN::kan*^{R}; pUT18C-*recA::carb*^{R}	BTH101 was co-transformed with pNABC495 ([6]) and pNABC492 for the bacterial-two-hybrid assay.
NABC508	CB15N; P_{xyl}-*ssb-YFP::kan*^{R}	CB15N was transformed with pNABC512 plasmid to integrate *ssb-YFP* linked to *kan*^{R} at the P_{xyl} locus.
NABC509	P_{lacI}-*lacI(hfa locus)*; P_{lac}-*dnaA(dnaA locus);* I-SceI site(after CCNA_00029)::*tet*^{R}; P_{van}-*I-SceI::chlor*^{R}*; mipZ-mCherry::gent*^{R}; P_{xyl}-*ssb-YFP::kan*^{R}	NABC461 was transduced with lysate of a strain harboring *ssb-YFP* linked to *kan*^{R} (NABC508) integrated at P_{xyl} locus. Resultant strain was transduced with lysate of a strain harboring *mipZ-mCherry* linked to *gent*^{R} (NABC451) integrated at endogenous locus. Finally, lysate of NABC439 was transduced to generate a *recN* deletion linked to *gent*^{R}.
NABC510	CB15N; *mipZ-mCherry::spec*^{R}	CB15N was transformed with pNABC513 plasmid to integrate *mipZ-mCherry* linked to *spec*^{R} at the endogenous locus.
NABC511	P_{lacI}-*lacI(hfa locus)*; P_{lac}-*dnaA(dnaA locus);* I-SceI site(after CCNA_00029)::*tet*^{R}; P_{van}-*I-SceI::chlor*^{R}*; mipZ-mCherry::spec*^{R}; P_{xyl}-*ssb-YFP::kan*^{R}*;ΔrecN::gent*^{R}	NABC461 was transduced with lysate of a strain harboring *ssb-YFP* linked to *kan*^{R} (NABC508) integrated at P_{xyl} locus. Resultant strain was transduced with lysate of a strain harboring *mipZ-mCherry* linked to *spec*^{R} (NABC510) integrated at endogenous locus. Finally, lysate of NABC439 was transduced to generate a *recN* deletion linked to *gent*^{R}.
NABC516	P_{lacI}-*lacI(hfa locus)*; P_{lac}-*dnaA(dnaA locus);* I-SceI site(after CCNA_00029)::*tet*^{R}; P_{van}-*I-SceI::chlor*^{R}; *Δsmc::kan*^{R} ; P_{xyl}-*recA-YFP::spec*^{R}	NABC464 was transduced with a lysate harbouring *recA-YFP* (NABC448) linked to *spec*^{R} integrated at the P_{xyl} locus.
NABC517	P_{lacI}-*lacI(hfa locus)*; P_{lac}-*dnaA(dnaA locus);* I-SceI site(after CCNA_00029)::*tet*^{R}; P_{van}-*I-SceI::chlor*^{R}; P_{xyl}-*recA-mCherry::gent*^{R}; *recN-YFP::spec*^{R}	NABC461 was transduced with a lysate harbouring *recA-mCherry* (NABC446) linked to *gent*^{R} integrated at the P_{xyl} locus. Resultant strain was transduced with a lysate harbouring *recN-YFP* (NABC449) linked to *spec*^{R}at the endogenous locus.
NABC518	BTH101; pKT25-*recN(E473Q)::kan*^{R}; pUT18C-*recA::carb*^{R}	BTH101 was co-transformed with pNABC495 ([6]) and pNABC521 for the bacterial-two-hybrid assay.
NABC519	BTH101; pKT25-*recN(D472A)::kan*^{R}; pUT18C-*recA::carb*^{R}	BTH101 was co-transformed with pNABC495 ([6]) and pNABC522 for the bacterial-two-hybrid assay.
NABC520	CB15N; *ΔlexA::tet*^{R} ; *ΔsidA::markerless*	([7])
NABC265	CB15N; *ΔlexA::tet*^{R}; *ΔsidA::markerless*; *ΔrecA::kan*^{R}	NABC520 was transduced with lysate of a strain harboring *recA* deletion (NABC444) andselected for *kan*^{R} that is linked to deletion.

NABC586	CB15N; *recN(E473Q)*	CB15N was transformed with pNABC491 plasmid to generate a specific mutation in the ATP hydrolysis domain of RecN through two-step recombination procedure.
NABC587	CB15N; *recN(K35A/E473Q)::kanR*	NABC587 was transformed with pNABC584 plasmid to generate a specific mutation in the ATP hydrolysis domain of RecN through two-step recombination procedure. The resultant strain was transformed with pNABC585 to link *recN(K35A/E473Q)* with kan^R.
NABC588	P_{lacI}-*lacI(hfa locus)*; P_{lac}-*dnaA(dnaA locus);* I-SceI site(after CCNA_00029)::tet^R; P_{van}-*I-SceI::chlor*^{R}; P_{xyl}-*recA-YFP::gent*^{R};	NABC461 was transduced with lysate of a strain harboring P_{xyl}-*recA-YFP* (NABC447) and selected for $gent^R$.
NABC589	P_{lacI}-*lacI(hfa locus)*; P_{lac}-*dnaA(dnaA locus);* I-SceI site(after CCNA_00029)::tet^R; P_{van}-*I-SceI::chlor*^{R}; P_{xyl}-*recA-YFP::gent*^{R}; *recN(K35A/E473Q)::kan*^{R}	NABC588 was transduced with lysate of a strain harboring *recN(K35A/E473Q)* (NABC587) and selected for kan^R.

References

1. Joseph, A. M., Daw, S., Sadhir, I. & Badrinarayanan, A. Coordination between nucleotide excision repair and specialized polymerase DnaE2 action enables DNA damage survival in non-replicating bacteria. *eLife* **10**, e67552 (2021).
2. Modell, J. W., Kambara, T. K., Perchuk, B. S. & Laub, M. T. A DNA Damage-Induced, SOS-Independent Checkpoint Regulates Cell Division in Caulobacter crescentus. *PLoS Biol.* **12**, e1001977 (2014).
3. Skerker, J. M., Prasol, M. S., Perchuk, B. S., Biondi, E. G. & Laub, M. T. Two-Component Signal Transduction Pathways Regulating Growth and Cell Cycle Progression in a Bacterium: A System-Level Analysis. *PLoS Biol.* **3**, e334 (2005).
4. Badrinarayanan, A., Le, T. B. K. & Laub, M. T. Rapid pairing and resegregation of distant homologous loci enables double-strand break repair in bacteria. *J. Cell Biol.* **210**, 385–400 (2015).
5. Karimova, G., Pidoux, J., Ullmann, A. & Ladant, D. A bacterial two-hybrid system based on a reconstituted signal transduction pathway. *Proc. Natl. Acad. Sci.* **95**, 5752–5756 (1998).
6. Badrinarayanan, A., Le, T. B. K., Spille, J.-H., Cisse, I. I. & Laub, M. T. Global analysis of double-strand break processing reveals in vivo properties of the helicase-nuclease complex AddAB. *PLOS Genet.* **13**, e1006783 (2017).
7. Modell, J. W., Hopkins, A. C., & Laub, M. T. (2011). A DNA damage checkpoint in Caulobacter crescentus inhibits cell division through a direct interaction with FtsW. *Genes & development*, **25**, 1328–1343.

Supplementary table 2: Plasmids used in present study

Plasmid name	Construct details/ Source	Antibiotic
pNPTS138	([1])	Kanamycin
pMCS-1	([2])	Spectinomycin
pMCS-4	([2])	Gentamycin
pMCS-2	([2])	Kanamycin
pCHYC-2	([2])	Kanamycin
pCHYC-4	([2])	Gentamycin
pXYFPC-1	([2])	Spectinomycin
pXCHYC-4	([2])	Gentamycin
pXCHYC-1	([2])	Spectinomycin
pXYFPC-4	([2])	Gentamycin
pRXMCS-6	([2])	Chloramphenicol
pRXMCS-2	([2])	Kanamycin
pXYFPC-2	([2])	Kanamycin
pCHYC-1	([2])	Spectinomycin
pNABC480	Full length *recA* was amplified from *C. crescentus* DNA usingAB281 and AB282, restriction digested with NdeI/KpnI and ligated to NdeI/KpnI digested pXYFPC-1 vector. Linker between RecA and YFP was 20 amino acid long.	Spectinomycin
pNABC481	Full length *recA* was amplified from *C. crescentus* DNA usingAB281 and AB282, restriction digested with NdeI/KpnI and ligated to NdeI/KpnI digested pXCHYC-4 vector. Linker between RecA and YFP was 20 amino acid long.	Gentamycin
pNABC482	pMCS-4 vector harboring CCNA_01139 from *C. crescentus* genome([3]).	Gentamycin
pNABC483	Full length *recN* was amplified from *C. crescentus* DNA usingAC251 and AC252, restriction digested with NdeI/EcoRI and ligated to NdeI/EcoRI digested pXYFPC-1 vector. Linker between RecN and YFP was 11 amino acid long.	Spectinomycin
pNABC484	Full length *recA* was amplified from *C. crescentus* DNA usingAB281 and AB282, restriction digested with NdeI/KpnI and ligated to NdeI/KpnI digested pXCHYC-1 vector. Linker between RecA and YFP was 20 amino acid long.	Spectinomycin
pNABC485	Full length *mipZ* was amplified from *C. crescentus* DNA usingAB332 and AB341, restriction digested with NdeI/KpnI and ligated to NdeI/KpnI digested pCHYC-2 vector. Linker between MipZ and mCherry was 20 amino acid long.	Kanamycin
pNABC486	Full length *mipZ* was amplified from *C. crescentus* DNA usingAB332 and AB341, restriction digested with NdeI/KpnI and ligated to NdeI/KpnI digested pCHYC-1 vector. Linker between MipZ and mCherry was 20 amino acid long.	Gentamycin
pNABC487	pXYFPC-4 vector backbone harboring full length *recA* from *C. crescentus* genome([3]).	Gentamycin
pNABC488	600bp downstream of CCNA_02067 was amplified from *C. crescentus* gDNA using AC95 and AC96, restriction digestedwith NdeI/KpnI and ligated to NdeI/KpnI digested pMCS-1 vector.	Spectinomycin

pNABC489	Last ~600bp of *recN* were amplified from *C. crescentus* gDNA using AB439 and AB445. *eyfp* was amplified from pXYFPC-1 using AB446 and AB447. Spectinomycin resistance cassette was amplified using AB363 and AB364. ~600bp downstream of *recN* was amplified from *C. crescentus* gDNA using AB365 and AB444. pNPTS138 vector was digested with BamHI/NheI. All amplified fragments and digested vector were assembled using Gibson assembly.	Spectinomycin
pNABC490	600bp upstream of the mutation site(D472) of *recN* was amplified using AC87 and AC89 from *C. crescentus* gDNA. 600bp downstream of the mutation site(D472) of *recN* was amplified using AC90 and AC88 from *C. crescentus* gDNA. pNPTS138 vector was digested with BamHI/NheI. The upstream fragment, downstream fragment and digested vectorwere assembled using Gibson assembly. AC89 and AC90 areoverlapping oligos which harbor the desired mutant sequence.AC270 and AC271 were used for confirming the mutated sequence.	Kanamycin
pNABC491	600bp upstream of the mutation site(E473) of *recN* was amplified using AC87 and AC91 from *C. crescentus* gDNA. 600bp downstream of the mutation site(E473) of *recN* was amplified using AC92 and AC88 from *C. crescentus* gDNA. pNPTS138 vector was digested with BamHI/NheI. The upstream fragment, downstream fragment and digested vectorwere assembled using Gibson assembly. AC91 and AC92 areoverlapping oligos which harbor the desired mutant sequence.AC270 and AC271 were used for confirming the mutated sequence.	Kanamycin
pNABC492	Full length *recN* was amplified from the *C. crescentus* gDNA using AB353 and AB354. The amplified fragment and pKT25were both digested with BamHI/KpnI and ligated to assemble the required construct.	Kanamycin
pNABC493	Full length *recN* was amplified from the *C. crescentus* gDNAusing AB353 and AB354. The amplified fragment and pUT18C were both digested with BamHI/KpnI and ligated to assemble the required construct.	Carbenicillin
pNABC494	pKT25 vector backbone harboring full length *recA* from *C. crescentus* genome([4]).	Kanamycin
pNABC495	pUT18C vector backbone harboring full length *recA* from *C. crescentus* genome([4]).	Carbenicillin
pNABC496	Full length *recA* was amplified from *C. crescentus* gDNAusing AB281 and AB282. The amplified fragment and pRXMC-6 were restriction digested with NdeI/KpnI and ligated to assemble required construct.	Chloramphenicol
pNABC497	An internal fragment of CCNA_01139 was amplified using AB271 and AB272 from *C. crescentus* gDNA. The above amplified fragment and pMCS-2 were restriction digested with NdeI/SacI and ligated to assemble the required construct.	Kanamycin
pNABC498	pRXMCS-2 vector backbone harboring *YFP* expressed under the P_{sidA} promotor ([5]).	Kanamycin
pNABC512	Full length *ssb* was amplified from *C. crescentus* DNA usingAB658 and AB659, restriction digested with NdeI/KpnI and ligated to NdeI/KpnI digested pXYFPC-1 vector. Linker between SSB and YFP was 20 amino acid long.	Kanamycin

pNABC513	Full length *mipZ* was amplified from *C. crescentus* DNA using AB332 and AB341, restriction digested with NdeI/KpnI and ligated to NdeI/KpnI digested pCHYC-1vector. Linkerbetween MipZ and mCherry was 20 amino acid long.	Spectinomycin
pNABC521	Full length *recN(E473Q)* was amplified by a colony PCR of a single colony of NABC453 using AB353 and AB354. The amplified fragment and pKT25were both digested with BamHI/KpnI and ligated to assemble the required construct.	Kanamycin
pNABC522	Full length *recN(D472A)* was amplified by a colony PCR of a single colony of NABC452 using AB353 and AB354. The amplified fragment and pKT25were both digested with BamHI/KpnI and ligated to assemble the required construct.	Kanamycin
pNABC584	600bp upstream of the mutation site(K35) of *recN* was amplified using AC240 and AC239 from *C. crescentus* gDNA. 600bp downstream of the mutation site(E473) of *recN* was amplified using AC238 and AC241 from *C. crescentus* gDNA. pNPTS138 vector was digested with BamHI/NheI. The upstream fragment, downstream fragment and digested vectorwere assembled using Gibson assembly. AC238 and AC239 areoverlapping oligos which harbor the desired mutant sequence.AC266 and AC287 were used for confirming the mutated sequence.	Kanamycin
pNABC585	600bp downstream of CCNA_02067 was amplified from *C. crescentus* gDNA using AC95 and AC96, restriction digestedwith NdeI/KpnI and ligated to NdeI/KpnI digested pMCS-2 vector.	Kanamycin

References

1. Skerker, J. M., Prasol, M. S., Perchuk, B. S., Biondi, E. G. & Laub, M. T. Two-Component Signal Transduction Pathways Regulating Growth and Cell Cycle Progression in a Bacterium: A System-Level Analysis. *PLoS Biol.* **3**, e334 (2005).
2. Thanbichler, M., Iniesta, A. A. & Shapiro, L. A comprehensive set of plasmids for vanillate- and xylose-inducible gene expression in Caulobacter crescentus. *Nucleic Acids Res.* **35**, e137–e137 (2007).
3. Badrinarayanan, A., Le, T. B. K. & Laub, M. T. Rapid pairing and resegregation of distant homologous loci enables double-strand break repair in bacteria. *J. Cell Biol.* **210**, 385–400 (2015).
4. Badrinarayanan, A., Le, T. B. K., Spille, J.-H., Cisse, I. I. & Laub, M. T. Global analysis of double-strand break processing reveals in vivo properties of the helicase-nuclease complex AddAB. *PLOS Genet.* **13**, e1006783 (2017).
5. Modell, J. W., Kambara, T. K., Perchuk, B. S. & Laub, M. T. A DNA Damage-Induced, SOS-Independent Checkpoint Regulates Cell Division in Caulobacter crescentus. *PLoS Biol.* **12**, e1001977 (2014).

Supplementary table 3: Oligos used in present study

Oligo	Sequence
AB281	TTATCATATGACAAGTCAGGCGGCTTTGAAACTCG
AB282	TTATGGTACCGTCCTCTTCGCCCTCTTCCGG
AC251	TCAGACGCTCGAGTTTTGGGGAGACGACCAATGCTGATCGGCCTTTCCATCCGTGACGT
AC252	GGTGGCCGACCGGTGACGCGTAACGTTGGCGTGAAGGGTCAGCAACGCCC
AB332	TTATCATATGGCCGAAACGCGCGTTATCG
AB341	TTATGGTACCCTGCGCCGCCAGCATCGT
AC95	TCCAATTGCATATGACCCGGCTGGAAAATGCTGTA
AC96	GATCTTAAGGTACCCGGCTTGCGTCCAGTCTTCG
AC87	CAAGCTTCTCTGCAGGATATCTGGGCTGTCGGCGGCCTGC
AC88	CGGAGACGCGTCACGGCCGAAGGCCTCGGACCTGTCTGGCGAAG
AC89	CTGATCCACCTCGGCGAAGATCATCAA
AC90	TTGATGATCTTCGCCGAGGTGGATCAG
AC91	CCTGATCCACCTGGTCGAAGATCATCAAC
AC92	GTTGATGATCTTCGACCAGGTGGATCAGG
AC270	GTTCCGCGTCGCTGTCGAACC
AC271	CTAGGCGTGAAGGGTCAGCAA
AB353	TTATGGATCCCATGCTGATCGGCCTTTCCATCC
AB354	TTATGGTACCCTAGGCGTGAAGGGTCAGCAACG
AB271	TTATCATATGGCCACCCATGACGCGGGC
AB272	TTATGAGCTCTTATGCCTTGCCGCCCTTGCTG
AB658	TTATCATATGGCTGGCAGCGTCAACAAGG
AB659	TTATGGTACCGAACGGGATCTCGTCGTCCAGATC
AB439	CAAGCTTCTCTGCAGGATATCTGAAGGACGCGGCTGAGGCG
AB445	CGACCGGTGACGCGTAACGTTGGCGTGAAGGGTCAGCAACG
AB446	AACGTTACGCGTCACCGGTCG
AB447	TTACTTGTACAGCTCGTCCATGCCGA
AB363	TCGGCATGGACGAGCTGTACAAGTAACCAGAACCTTGACCGAACGCAG
AB364	CTAGATGCCGACTACCTTGGTGATCTCG
AB365	CCAAGGTAGTCGGCATCTAGAGCCTGTCTGGTTTAGATGGAACTATCTAAACCAG
AB444	CGGAGACGCGTCACGGCCGAAGCGCTCAGGGGCCCAATACG
AC239	GGATGATCGACGCGCCCGCCCCG
AC240	CAAGCTTCTCTGCAGGATATCTGGACGCGCGGCTGAAGATCGACATG
AC238	CGGGGCGGGCGCGTCGATCATCC
AC241	CGGAGACGCGTCACGGCCGAAGGCCGGCCAGCGCATCCTGAGC
AC266	ATGCTGATCGGCCTTTCCATC
AC287	CGCGAACGACCGTCGGGC